PHYSICAL REVIEW B **85**, 245451 (2012)

Competing nematic, antiferromagnetic, and spin-flux orders in the ground state of bilayer graphene

Y. Lemonik and I. Aleiner
Physics Department, Columbia University, New York, New York 10027, USA

V. I. Fal'ko
Physics Department, Lancaster University, Lancaster LA1 4YB, UK

(Received 20 March 2012; revised manuscript received 4 June 2012; published 29 June 2012)

We analyze the phase diagram of bilayer graphene (BLG) at zero temperature and zero doping. Assuming that at high energies the electronic system of BLG can be described within a weak-coupling theory (consistent with the experimental evidence), we systematically study the evolution of the couplings with going from high to low energies. The divergences of the couplings at some energies indicate the tendency towards certain symmetry breakings. Carrying out this program, we found that the phase diagram is determined by microscopic couplings defined on the short distances (initial conditions). We explored all plausible space of these initial conditions and found that the three states have the largest phase volume of the initial couplings: nematic, antiferromagnetic, and spin flux (a.k.a. quantum spin Hall). In addition, ferroelectric and two superconducting phases appear only near the very limits of the applicability of the weak-coupling approach. The paper also contains the derivation and analysis of the renormalization group equations and the group theory classification of all the possible phases which might arise from the symmetry breakings of the lattice, spin rotation, and gauge symmetries of graphene.

DOI: 10.1103/PhysRevB.85.245451 PACS number(s): 73.22.Pr, 73.21.−b

I. INTRODUCTION

Bilayer graphene[1,2] (BLG) is a crystal which consists of two monolayers of honeycomb carbon lattice arranged according the Bernal stacking known from bulk graphite.[2] In a Bernal-stacked lattice, one out of the two sites on the upper monolayer resides directly over a site on the lower lattice, and the other carbon atoms are on/under the centers of the hexagons (see Fig. 1). Such a crystal has a very high symmetry with symmetry group $\mathcal{D}_{3d}$.

This high symmetry may be lifted by the formation of correlated states of electrons. There is a plethora of ways the symmetry can be lifted, some of which have been discussed in the recent literature: the ferroelectric-layer asymmetric state,[3,4] the layer polarized antiferromagnetic state,[5–8] the quantum anomalous Hall state,[4,7,9] the "spin flux"/quantum spin Hall state,[4,7] the charge density wave state,[7,10,11] the loop current state,[12] and an anisotropic nematic liquid.[13,14] Some of the proposed phases above have a gap in the electronic spectrum (ferroelectric, antiferromagnetic, spin flux, CDW), whereas in the other phases (nematic, ferromagnetic) no gap is formed. This large variety of possibilities makes the theory of electronic properties of BLG a very interesting and challenging subject. The complexity of the theoretical problem is compounded by two factors. One is a lack of precise information about the relevant interaction constants which determine the electronic phase in undoped pristine BLG. The other issue is the competition between exchange energy contributions for a large number of candidate phases which makes the determination of the ground state nontrivial, even with precise knowledge of the interaction constants.

On the experimental side, several contradicting observations have been reported based on interpretations of the measured transport properties of suspended samples in terms of a gapful or gapless spectrum of electronic excitations.[15–21] At the moment the preponderance of experiments point to a gapped state, but a lack of consistency between samples and between experiments means there is not a yet a clear understanding of the situation. However, all of these works as well as optical studies of BLG[22–27] indicate that the high-energy properties (but below 0.2 eV) of BLG are well described by the two-band model[1] without interactions. All this makes a comprehensive theoretical treatment of the problem starting from the weak coupling well-defined and timely. In this paper, we employ the previously developed RG approach[13] to identify the possible scenarios of the symmetry breaking phase transition in BLG at low temperature and zero carrier density.

The tendency to form a state with spontaneously broken symmetry is encoded in the system response to local symmetry breaking fluctuations, in particular in their mutual interaction,

$$H_{\text{int}} \sim \int d^2 r \sum_{\mathcal{A}\in\text{IrReps}} g_{\mathcal{A}} \delta\hat{\rho}_{\mathcal{A}}(r) \cdot \delta\hat{\rho}_{\mathcal{A}}(r). \qquad (1.1)$$

Here $\delta\hat{\rho}_{\mathcal{A}}$ are operators creating local density fluctuations breaking lattice symmetry, with $\delta\hat{\rho}_{\mathcal{A}} = \psi^\dagger \hat{M} \psi$ expressed in terms of electron annihilation and creation operators ψ and $\psi^\dagger$, and $g_{\mathcal{A}}$ are coupling constants. Each of the fluctuations $\delta\hat{\rho}_{\mathcal{A}}$ belong to one of the irreducible representations $\mathcal{A}$ (IrReps) of the symmetry group of the lattice. (A precise definition of the densities can be found in Sec. II.)

If Hamiltonian (1.1) is dominated by one term with negative constant $g_{\mathcal{A}}$, we would expect it to be energetically favorable for a state with a nonzero expectation value of $\delta\hat{\rho}_{\mathcal{A}}$ to form, with the symmetry of the ground state determined by the corresponding IrRep, $\mathcal{A}$. However if the coupling constant in the dominant term is positive, then the ground state is determined by the exchange energy, which can be negative not only for magnetic (ferro/antiferro) but also for nonmagnetic orderings, because of the sublattice/valley matrix structure. Because of the large number of IrReps, this can result in a competition between many phases. Therefore, to determine the ground state of BLG we must know all the interaction

 ©2012 American Physical Society

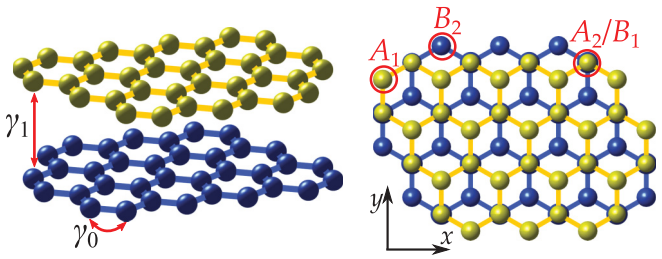

FIG. 1. (Color online) Left panel: 3D view of bilayer graphene. The sites that sit on top of each other, connected by dotted lines, hybridize strongly and form bands with a gap of $\gamma_1 \approx 0.4$ eV. The low-energy electrons live on the half of the carbon atoms that sit over/under the centers of the hexagons. Right panel: Top-down view of the lattice.

constants $g_{\mathcal{A}}$ sufficiently well, especially when the dominant ones are positive. The situation is actually even more intriguing since attraction may result in a superconducting phase with nontrivial Cooper pair structure.

To add to the complexity of the problem, the values of the "constants" $g_{\mathcal{A}}$ are not fixed. They change as a function of the energy scale $\mathcal{E}$ within which the electrons establish the symmetry breaking correlations. The energy scale dependence, $g_{\mathcal{A}}(\mathcal{E})$, may be calculated using the renormalization group (RG) approach. In the RG approach the highest energy electron states are eliminated and their effects incorporated into a redefinition of the parameters of the theory. The renormalization of BLG parameters starts at the energy scale $\gamma_1/2 \approx 0.2$ eV which limits the applicability of the two-band model with parabolic spectrum and initial conditions $g_{\mathcal{A}}(\gamma_1/2)$. Then it is iterated until the lowest energy scale $\mathcal{E}$ is reached. This energy scale $\mathcal{E}$ is determined when the interaction energy in at least one of the the channels becomes of the order of kinetic energy. After this scale is reached the mean-field theory can be used to establish the electronic ground state. The necessary RG equations for the constants $g_{\mathcal{A}}$ and their interplay with Coulomb interaction,

$$H_C \sim \int d^2r d^2r' \frac{\psi^\dagger(r)\psi(r)\psi^\dagger(r')\psi(r')}{|r-r'|}, \qquad (1.2)$$

have been derived for the full set of eight constants in Ref. 13. [Similar in spirit the treatment of Ref. 8 replaced Eq. (1.2) with the short-range weak interaction.]

Calculating $g_{\mathcal{A}}(\gamma_1/2)$ requires detailed knowledge of the microscopic orbitals which is not available at present. Therefore, in this paper we explore a wide variety of initial conditions $g_{\mathcal{A}}(\gamma_1/2)$ for the RG to find possible electronic ground states for BLG. We can make some arguments to constrain the values of the $g_{\mathcal{A}}(\gamma_1/2)$. The coupling g_{B_2} which describes the interaction of dipoles oriented perpendicular to the bilayer (see Fig. 2) must be positive at high energy scales. The four "current-current" interactions g_{A_2}, g_{B_1}, g_{E_1}, and $g_{E_1''}$ are only generated by virtual processes because of time reversal symmetry. Therefore we will set them to be zero at $\gamma_1/2$.

Also, it is interesting to note that in the value of $g_{\mathcal{A}}(\gamma_1/2)$ one has to take account of the interactions between electrons via polarization of the lattice. Particularly, the in-plane TO-LO phonons at the Γ point and TO phonons at the Brillouin zone corner have energies comparable to $\gamma_1/2$, so that they mediate an attractive interaction via their virtual creation/absorption. These would give negative contributions to the bare values of g_{E_2} and $g_{E_2''}$. Analogously, virtual LO-LA phonons from K—the Brillouin zone corners—give negative contribution to the value of g_G. Therefore, we make no assumption about the sign of g_{E_2}, $g_{E_2''}$, and g_G. A set of typical outcomes of the RG flow and the resulting electronic phases is shown in Fig. 3.

In Fig. 3 we reproduce the earlier reported result[13,14] that for the initial choice of $g_{\mathcal{A}} = 0$ the RG flow leads to a nematic phase. The nematic phase is a state with broken rotational (but intact translational) symmetry corresponding to representation E_2 in Fig. 2, mimicking the effect of anisotropic hopping along bonds with different directions on the honeycomb lattice. This

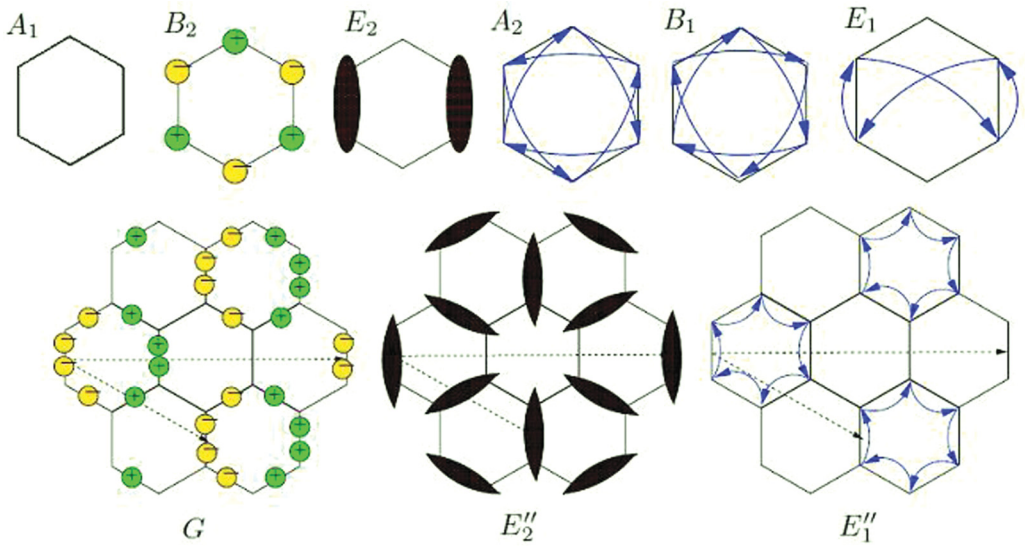

FIG. 2. (Color online) Sketches of the density and currents transforming according representations of the group $\mathcal{D}_{3d}''$. In the case of a spin singlet symmetry breaking, the plus and minus signs represent charges, the blue lines represent persistent currents, and the black bars represent bonds. The G, E_2, and E_2'' order parameters triple the unit cell; the new Bravais lattice vectors are given by the dashed arrows. The representations are given in terms of Pauli matrices in Eqs. (2.11) and (2.10).

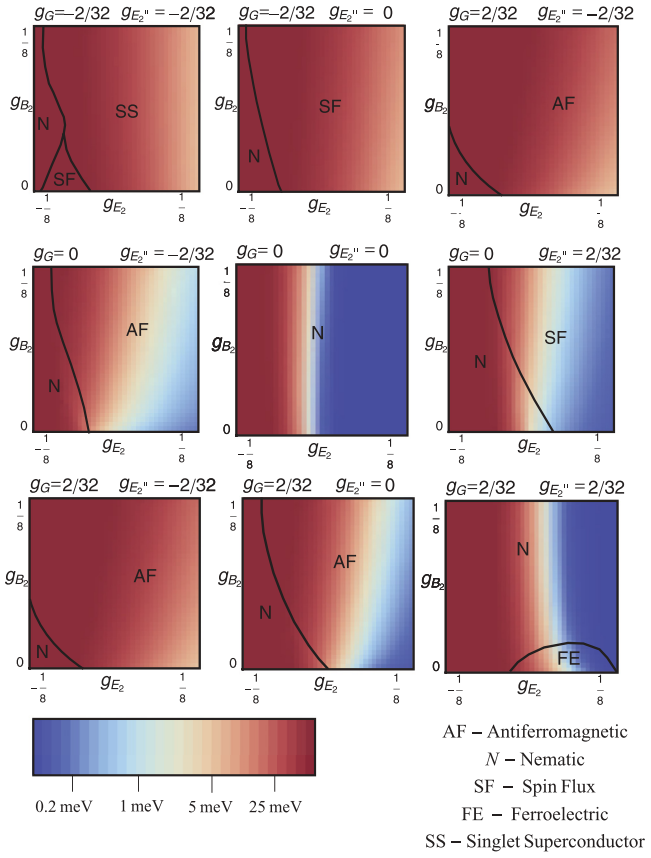

FIG. 3. (Color online) Four cuts through the possible parameter space of BLG. The predicted gap (or saddle point energy for only gapless nematic phase) is indicated by the color scale and the predicted phase is indicated. N is a nematic, AF is an antiferromagnetic phase, SF is a spin flux phase, and FE is a ferroelectric. A fifth predicted superconducting phase is in a range parameters not shown; see Fig. 9 for more details. The g are coupling constants of BLG, with the subscript labeling the irreducible representations in accordance with Fig. 2 and defined in Sec. II. All boundaries are the first-order phase transitions.

breaks the sixfold rotational symmetry by selecting one of axes of the lattice. In this state the electronic spectrum remains gapless but is significantly reconstructed from the unbroken symmetry state with two fourfold degenerate Dirac cones at low energy. The state has the same symmetry and spectrum as uniaxial strain,[28] and we expect that strain will, all else equal, favor the nematic phase. Figure 3 shows that the nematic phase is the preferred ground state not only when $g_{\mathcal{A}}(\gamma_1/2) = 0$, but in a significant section of the $g_{\mathcal{A}}(\gamma_1/2)$ parameter space. In particular, the nematic phase always emerges from the part of the parameter space where bare electron-electron couplings causing intervalley scattering are zero ($g_G = g_{E_2''} = g_{E_1''} = 0$).

In other parts of the parameter space explored in this work and illustrated in Fig. 3, the ground state appears to be antiferromagnetic (AF), with the A_1 and B_2 sublattices of two layers, see Fig. 1, spin polarized in opposite directions. In the AF state the electronic excitations are gapped (though neutral spin wave excitations are gapless). Although the AF state prevails over a significant section of the parameter space, the combinations of bare couplings which produce the AF state are not intuitive. For example, increasing the bare coupling g_{B_2} does not necessarily introduce the AF phase. However increasing the bare coupling g_G makes the ground state AF. The reason for this counterintuitive behavior is in the complexity of the RG flows. Since there are eight nonlinearly coupled variables in the RG equations,[8,13] the RG flow is quite complicated, and the connection between the couplings at low energy and the bare couplings at high energy is not obvious.

Exploring a broader parameter space further we find more phases. A spin-flux phase is found in a significant sector of the parameter space $g_{\mathcal{A}}(\gamma_1/2)$, as seen in Fig. 3. This spin-flux phase is a state with a persistent spin current circling the honeycomb lattice rings, corresponding to the spin triplet form of representation B_1 in Fig. 2. It may be viewed as the spontaneous formation of a strong spin-orbit coupling. It therefore leads to a gapped electronic spectrum and possibly a quantum spin Hall effect.

There are two more phases which appear to some degree in the phase space explored. One is a ferroelectric phase (FE). The FE phase a trivial band gap insulator where the bilayer becomes spontaneously charged like a capacitor. It is a completely gapped phase. It corresponds to representation B_2, precisely the same representation as AF but spin singlet, rather than spin triplet. Therefore, positive g_{B_2} suppresses the ferroelectric phase, which appears in Fig. 3 only in the fine-tuned corners corresponding to the applicability of the weak-coupling theory.

We also found a new superconducting phase (not shown in the figure; see Fig. 9 for more details) which has energy tantalizingly close to the nematic and ferroelectric states. It is a triplet superconductor with a nontrivial Cooper pairing. Cooper pairs are formed between pairs of electrons with opposite valleys and opposite layer. The pairing is symmetric in exchange of valleys, but antisymmetric in exchange of layers.

As usual, the singlet superconductivity appears only for the attractive interaction. From the first panel on Fig. 3, we see that it requires quite significant attraction in two channels $g_{E_2''}, g_G < 0$.

Below we describe how the conclusions listed above have been reached. In Sec. II we review the structure of BLG, its symmetry group, and the low-energy Hamiltonian. Section III describes the resummation of the Coulomb interactions in the $1/N$ expansion,[13,29–31] where $N = 4$ is the degeneracy of the single-particle spectrum. We then derive the RG equations that connect the couplings at low and high energy scales. In Sec. IV the results of the RG flow equations are analyzed and augmented by a self-consistent mean-field theory which produces a possible phase. Section V discusses the properties of the emerging phases. In the Appendix we describe the group-theoretic analysis of the phases of the BLG diagram.

II. MODEL

The top view of the BLG lattice with Bernal stacking is shown in the right panel of Fig. 1. Here we label the two layers 1 and 2 and the four inequivalent lattice sites A_1, B_1, A_2, B_2, with A_2 directly over B_1.

Calculation based on the minimal tight-binding model has established the following BLG band structure.[1] The A_2 and B_1 sites hybridize strongly and host states from the high-energy

bands with excitation energies $>\gamma_1 \approx 0.4$ eV. The low-energy fermionic excitations in BLG belong to a four-component representation of the group $\mathcal{D}_{3d}$, exactly as in monolayer graphene. The four fermionic fields ψ are conveniently joined into a 4-vector as follows:

$$\vec{\psi}^t \equiv \left\{\left(\psi_K^A, \psi_K^B\right)^{AB}, \left(\psi_{K'}^B, -\psi_{K'}^A\right)^{AB}\right\}_{KK'}, \tag{2.1}$$

where the ψs are true spinors including real electron spin. This four-dimensional space can be written as the direct product of the (AB) and (KK') spaces. We will use this to write all operators as the sum of direct products $\tau_a^{AB}\tau_b^{KK'}\sigma_c$ of Pauli matrices in each space. We define $\{\tau_i^{AB}, \tau_i^{KK'}, \sigma_i\}$ as the Pauli matrices acting on layer, valley, and spin, respectively, and define $\tau_0 \equiv \mathbb{1}$, $\tau_\pm \equiv (\tau_x \pm i\tau_y)/2$.

The symmetries of the BLG lattice consist of the two independent lattice translations $\hat{t}_1$ and $\hat{t}_2$, a $\hat{C}_3$, rotation by $2\pi/3$ around one of the lattice sites; and two independent reflections: $\hat{R}_h$, reflection across the y axis, and $\hat{R}_v$, reflection across the x axis, together with reflection through the plane midway between the graphene sheets; see the right panel of Fig. 1. The reflections and rotations form the point group $\mathcal{D}_{3d}$. The groups $\mathcal{D}_{3d}$ and $\mathcal{C}_{6v}$ are isomorphic and have precisely the same action on the plane. We also ignore the spin-orbit interaction which gives an additional SU(2) symmetry from the independent rotation of the spin. We will be concerned with the physics about K and K' points which are inequivalent in the Brillouin zone but are connected by $\hat{R}_h$. Rather than dealing with two degenerate but inequivalent points we can triple the unit cell, which maps K and K' onto the Γ point. In this view, the point group D_{3d} is expanded to $\mathcal{D}''_{3d} = \mathcal{D}_{3d} + \hat{t}_1\mathcal{D}_{3d} + \hat{t}_2\mathcal{D}_{3d}$ with the translation operator $\hat{t}_1$ with $\hat{t}_1^2 = \hat{t}_2$ and $\hat{t}_1^3 = \hat{1}$ (see, e.g., Ref. 32).

Ignoring the spin structure, the vector ψ transforms as follows under the action of the symmetry operators:

$$\begin{aligned}
\hat{t}_1\psi(\boldsymbol{r}) &= \exp\left(\frac{2\pi i}{3}\tau_z^{KK'}\right)\psi\left(t_1\boldsymbol{r}\right),\\
\hat{C}_3\psi(\boldsymbol{r}) &= \exp\left(\frac{4\pi i}{3}\tau_z^{AB}\right)\psi\left(C_3\boldsymbol{r}\right),\\
\hat{R}_h\psi(\boldsymbol{r}) &= \tau_y^{AB}\tau_y^{KK'}\psi\left(R_h\boldsymbol{r}\right),\\
\hat{R}_v\psi(\boldsymbol{r}) &= \tau_x^{AB}\tau_z^{KK'}\psi\left(R_v\boldsymbol{r}\right).
\end{aligned} \tag{2.2}$$

There is also the time reversal symmetry operation given by

$$\psi \to \psi^\dagger\hat{\mathcal{T}}; \quad \hat{\mathcal{T}} \equiv i\hat{\tau}_y^{AB}\hat{\tau}_y^{KK'}\hat{\sigma}_y. \tag{2.3}$$

A. Single-particle spectrum

We write the Hamiltonian for this model as

$$H \equiv H_0 + H_C + H_{\text{int}}. \tag{2.4}$$

The single-particle part of the Hamiltonian in the two-band model[1] reads (we will put $\hbar = 1$ in all the subsequent formulas)

$$H_0 \equiv \sum_k \psi^\dagger\left[\frac{1}{2m}\tau_z^{KK'}\left(\tau_+^{AB}k_+^2 + \tau_-^{AB}k_-^2\right)\right]\psi. \tag{2.5}$$

Here we ignore the "warping term"[1] caused by the small skew hopping (γ_3) since it would have a negligible effect on the RG. We have defined $k_\pm = k_x \pm ik_y$ and $m = 2\gamma_1/gr_{AB}^2\gamma_0^2$ where γ_0 is the the interlayer integral and r_{AB} is the interatomic distance. (The effect of the electron-electron interaction on the warping was studied in Ref. 13.) The Hamiltonian in Eq. (2.5) has the eigenvalue spectrum,

$$\varepsilon(\boldsymbol{k}) = \pm\frac{k^2}{2m}, \tag{2.6}$$

where each branch is fourfold (spin and valley) degenerate. The system described by Hamiltonian (2.5) has a higher symmetry than the underlying lattice. This larger symmetry is described by the SU(4) $\otimes$ $U(1)$ group whose sixteen generators M_{ij} are given by

$$M_{ij} = \sigma_i\tilde{\tau}_j^{KK'} \quad (i,j = 0,x,y,z), \tag{2.7}$$

$$\begin{aligned}
&\tilde{\tau}_0^{KK'} = \tau_0^{KK'}; \quad \tilde{\tau}_z^{KK'} = \tau_z^{KK'},\\
&\tilde{\tau}_x^{KK'} = \tau_z^{AB}\tau_x^{KK'}; \quad \tilde{\tau}_y^{KK'} = \tau_z^{AB}\tau_y^{KK'}.
\end{aligned} \tag{2.8}$$

An additional rotational $U(1)$ symmetry extends the discrete rotation $\hat{C}_3$ to a continuous transformation given by $\psi(\boldsymbol{r}) \to \exp(-2i\theta\sigma_z^{AB})\psi(\hat{R}(\theta)\boldsymbol{r})$, where $\hat{R}(\theta)$ is the real-space rotation by an angle θ.

The preceding discussion actually undercounts the symmetry algebra of the single-particle Hamiltonian greatly, since they do not include the continuous particle-hole symmetry rotations.[33] Including these rotations, the total symmetry group is $Sp(8)$. However these extra rotations are not necessary for the following analysis.

B. Electron-electron interactions

The Coulomb interaction,

$$H_C \equiv \frac{e^2}{2}\int\frac{d^2\mathbf{r}d^2\mathbf{r}'}{|\mathbf{r}-\mathbf{r}'|}[(\psi^\dagger\psi)_{\mathbf{r}}(\psi^\dagger\psi)_{\mathbf{r}'}], \tag{2.9}$$

is the largest interaction energy in the system. The strength of Coulomb interaction on the length scale L is e^2/L. The electron kinetic energy related to the same energy scale is $1/(mL^2)$ so the Coulomb interaction will dominate at the scale $L = 1/(me^2)$, which is comparable to the Bohr radius. However due to the generation of electron-hole pairs, the Coulomb interaction is screened, leading to the reduction of interaction energy $e^2/L \to 1/(mNL^2)$. This screened interaction respects all the symmetries of the system and does not scale; therefore by itself it does not induce any spontaneous symmetry breaking of the lattice symmetry group. We will return to the quantitative description of the screened Coulomb interaction in Sec. III.

Any lattice symmetry breaking is captured by the scaling of the marginal short-range interactions. These interactions also reduce the symmetries of the low-energy model almost down to the crystal group,[13,30,31,34]

$$H_{\text{int}} \equiv \frac{2\pi}{m}\int d^2\mathbf{r}\sum_{ij}g_{ij}\left[\psi^\dagger\hat{\tau}_i^{AB}\hat{\tau}_j^{KK'}\psi\right]_{\mathbf{r}}^2, \tag{2.10}$$

where have included a factor of $2\pi/m$ to make the couplings dimensionless. The $\mathcal{D}''_{3d}$ symmetry of the two-band BLG model

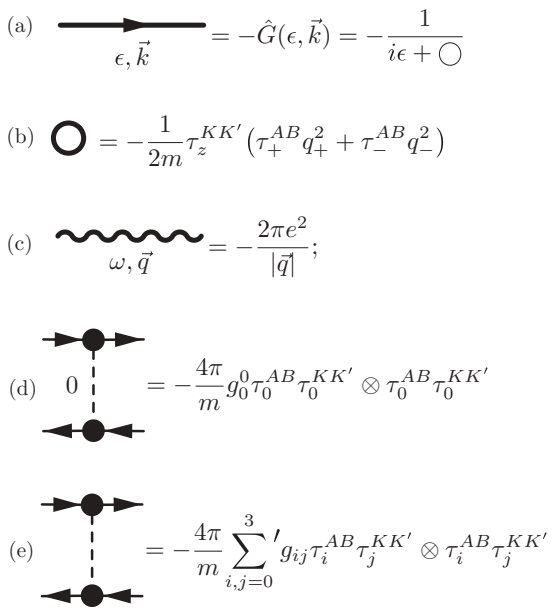

FIG. 4. Definition of the elements of the diagrammatic expansion. The thick line is the fermion propagator; the circle is the self-energy from the single particle of the spectrum. The wavy line is the Coulomb propagator and the dotted line is the contact interaction. We separate the scalar contact interaction g_{00} from the other interactions.

forces various relations among the g_{ij}:

$$\begin{aligned} &g_{xx} = g_{xy} = g_{yx} = g_{yy} \equiv g_G, \\ &g_{xz} = g_{yz} \equiv g_{E_2}; \quad g_{zx} = g_{zy} \equiv g_{E_2''}, \\ &g_{x0} = g_{y0} \equiv g_{E_1}; \quad g_{0x} = g_{0y} \equiv g_{E_1''}, \\ &g_{z0} \equiv g_{B_1}; \quad g_{0z} \equiv g_{A_2}; \quad g_{zz} \equiv g_{B_2}. \end{aligned} \tag{2.11}$$

Here we have labeled the couplings by the appropriate representation of $D_{3d}^{''}$ schematically represented in Fig. 2. We note for future reference that the interaction terms $g_{E_2}(\psi^\dagger\tau_{x,y}^{AB}\tau_z^{KK'}\psi)^2$ and $g_{B_1}(\psi^\dagger\tau_z^{AB}\psi)^2$ are invariant under the entire $U(4)$ [and which can be extended to $Sp(8)$ by including the particle-hole rotations[33]] symmetry of H_0. All other short-range interactions, such as those of the form $\sim(\psi_\mu^\dagger\vec{\sigma}_{\mu\nu}\psi_\nu)^2$ or $\sim|\psi_\mu^\dagger\psi_\nu^\dagger|^2$ can be always rearranged into the form of $H_{\rm int}$ by using standard Pauli matrix identity $2\delta_{\mu\nu}\delta_{\mu'\nu'} = \delta_{\mu\mu'}\delta_{\nu\nu'} + \vec{\sigma}_{\mu\mu'}\vec{\sigma}_{\nu'\nu}$.

III. PERTURBATION THEORY AND RG EQUATION

A. $1/N$ resummation

For the Coulomb interaction we will use $1/N$ as a small parameter, where $N = 4$ is the number of degenerate fermion flavors.[13,29–31] The elements of the diagrammatic expansion are defined on Fig. 4. We achieve 1/N expansion by performing the usual RPA resummation of diagrams (Fig. 5). Note that the coupling g_{00} has the same matrix structure as the long-range Coulomb interaction. We therefore resum the two together; i.e., we take the bare interaction in the RPA resummation to be

$$\mathcal{V}^{(0)}(q) \equiv \frac{2\pi e^2}{|q|} + \frac{4\pi g_{00}}{m}. \tag{3.1}$$

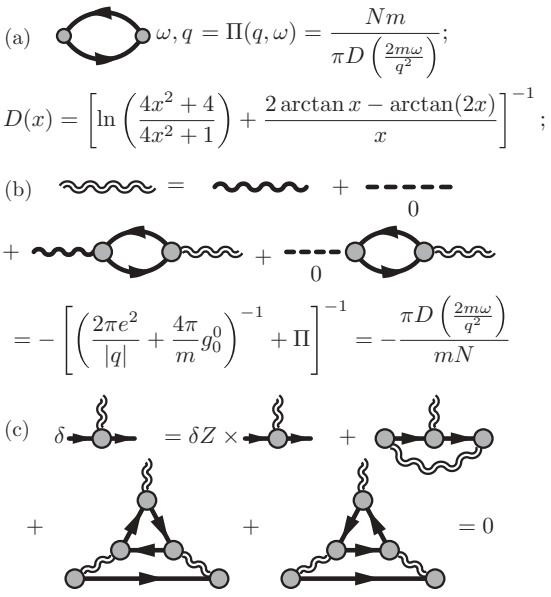

FIG. 5. Resummation of the strong Coulomb interaction in the $1/N$ approximation. (a) Evaluation of the polarization loop. (b) Definition of the resummed propagator, represented by the double wavy line. The scalar contact interaction is included in the resummation as it has the same matrix structure as the Coulomb interaction. (c) The non-renormalization of the Coulomb vertex as a result of gauge invariance. [δZ is defined in Fig. 6(a).]

Summing up the geometric series of terms in Fig. 5(b) we arrive at the resummed propagator,

$$\mathcal{D}(q,\omega) = \frac{\mathcal{V}^{(0)}(q)}{1 + \mathcal{V}^{(0)}(q)\Pi(q,\omega)}, \tag{3.2}$$

where

$$\begin{aligned} \Pi(q,\omega) &= \frac{mN}{\pi f\left(\frac{2m\omega}{q^2}\right)}, \\ f(x) &\equiv \left[\ln\left(\frac{x^2+1}{x^2+1/4}\right) + \frac{2\arctan x - \arctan 2x}{x}\right]^{-1}. \end{aligned} \tag{3.3}$$

We further take the long-wavelength limit, $q \to 0$, where $V^{(0)}(q)\Pi \gg 1$. This gives us the approximate expression for the interaction propagator,

$$\mathcal{D}(q,\omega) \approx \frac{1}{\Pi(q,\omega)} = \frac{\pi}{mN} f\left(\frac{2m\omega}{q^2}\right). \tag{3.4}$$

Since $\mathcal{D} \propto 1/N$ we can use a perturbative expansion in $1/N$. Note that we have neglected the higher energy bands in considering the resummation of the Coulomb potential. However, the higher energy bands would only change the dielectric constant which cancels out of the final formula.

Now we write the partition function as a path integral in imaginary time t over Grassman fields ψ and $\psi^\dagger$,

$$\begin{aligned} Z &= \int D\psi D\psi^\dagger e^{-S}, \\ S &\equiv \int d^2r dt \left(\psi^\dagger\frac{d}{dt}\psi - H[\psi^\dagger,\psi]\right), \end{aligned} \tag{3.5}$$

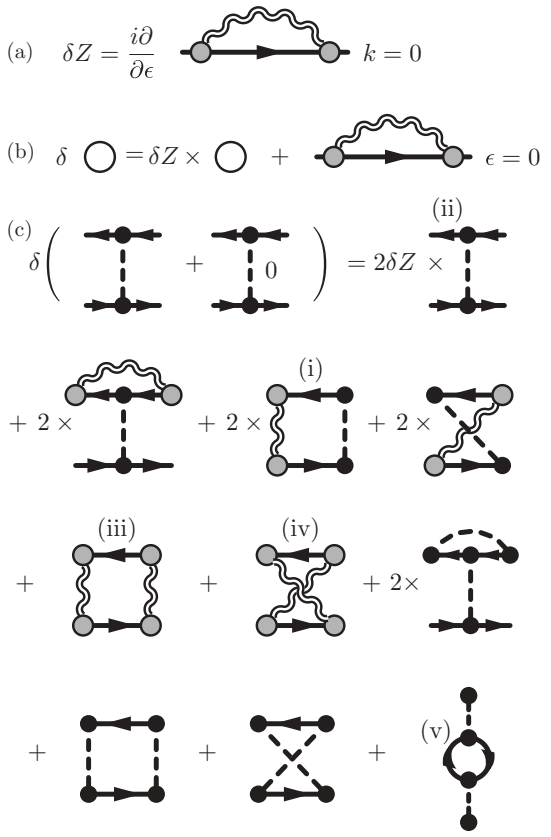

FIG. 6. Diagrams included in RG equations. (a) Single-particle particle weight renormalization. (b) Renormalization of the mass m. (c) Renormalization of the contact interactions.

where H is defined in Eq. (2.4). Then, we perform the RG by integrating out all fermionic states with momenta q such that $K > |q| > K\,e^{-\ell}$, where K is some ultraviolet cutoff regardless of ω. We will set K_0 so that $K_0^2/(2m) = \gamma_1/2$, approximately the upper limit of the applicability of the two-band model with the parabolic dispersion. We then rescale $\psi \to (1 + \delta Z/2)\psi$ to keep the term $\int \psi^\dagger \frac{d}{dt}\psi$ unchanged. This procedure has the benefit of not renormalizing the Coulomb vertex because of gauge invariance [see Fig. 5(c)]. If we assign t an RG dimension 2 then at tree level the operator ψ has RG dimension $+1$, and m, g_{ij}, and the Coulomb interaction are marginal.

There is a subtlety in the $1/N$ treatment of the Coulomb interaction. Because of the behavior of the interaction in the limit $q \to 0, \omega \to \infty$, some of the diagrams taken individually diverge faster than logarithmically. For example, the self-energy diagram [see Fig. 6(a)] gives the correction to the quasiparticle weight,

$$\begin{aligned}\delta Z &= \frac{\partial}{i\partial\Omega}\bigg|_{\Omega=0}\int \frac{d\omega d^2\boldsymbol{k}}{(2\pi)^3}\left(\frac{-\pi}{mN}\right) f\left(\frac{2m\omega}{k^2}\right)\\ &\quad\times\left[\frac{-i(\omega+\Omega)+\hat{\tau}_z^{KK'}(\hat{\tau}_+^{AB}k_+^2+\hat{\tau}_-^{AB}k_-^2)}{(\omega+\Omega)^2+\left(\frac{k^2}{2m}\right)^2}\right]\\ &= \frac{1}{N}\ln K\int_{-\infty}^{\infty}\frac{dx}{2\pi}f(x)\frac{1-x^2}{(1+x^2)^2},\end{aligned} \tag{3.6}$$

where the variable x is defined by the substitution $\omega = xk^2/(2m)$. This integral is formally infinite since $f(x) \to x$ as $x \to \infty$. To understand this divergence, note that it comes from the region where the momentum k through the Coulomb line goes to zero. This corresponds to a spatially constant but time-varying potential $V(t)$. Such a potential is merely a constant shift in energy so that the Green's function is changed as $G(t_1,t_2) \to G(t_1,t_2)\exp[ie\int_{t_1}^{t_2} V(t)\,dt]$. It is the summation over the fluctuations of this phase that produces the divergence. However, in all observable gauge-invariant quantities the fermion lines must come in closed loops which cancels out this phase, and so it cannot appear in any physical quantities. Reassuringly in all our calculations this is the case. Indeed such a divergence cancels out from the correction to the electron mass,

$$\delta\left(\frac{1}{2m}\right) = \frac{1}{2}\frac{\partial^2}{\partial p_+^2}\Sigma - \frac{1}{2m}\delta Z, \tag{3.7}$$

where

$$\begin{aligned}\frac{\partial^2}{\partial p_+^2}\Sigma &= \mathrm{tr}\left\{\frac{1}{2}\hat{\tau}_z^{KK'}\hat{\tau}_-^{AB}\frac{\partial}{\partial p_+^2}\bigg|_{p=0}\int\frac{d\omega d^2\boldsymbol{k}}{(2\pi)^3}\frac{\pi}{mN}\left[-f\left(\frac{2m\omega}{k^2}\right)\right]\hat{G}(\omega,\boldsymbol{k}+\boldsymbol{p})\right\}\\ &= -\mathrm{tr}\left\{\frac{1}{2}\hat{\tau}_z^{KK'}\hat{\tau}_-^{AB}\frac{\partial}{\partial p_+^2}\bigg|_{p=0}\int\frac{d\omega d^2\boldsymbol{k}}{(2\pi)^3}\frac{\pi}{mN}f\left(\frac{2m\omega}{k^2}\right)\frac{-i\omega+\frac{1}{2m}\hat{\tau}_z^{KK'}[\hat{\tau}_+^{AB}(k_++p_+)^2+\hat{\tau}_-^{AB}(k_-+p_-)^2]}{\omega^2+\left[\frac{(\boldsymbol{k}+\boldsymbol{p})^2}{2m}\right]^2}\right\}\\ &= -\int\frac{d^2k}{(2\pi)^2}\frac{1}{k^4}\int\frac{dx}{2\pi}\frac{\pi f(x)}{mN}\frac{\partial}{\partial p_+^2}\bigg|_{p=0}\frac{k_+^2+2k_+p_++p_+^2}{x^2+\left(1+\frac{k\cdot p}{k^2}+\frac{p^2}{k^2}\right)^2} = -\frac{1}{2mN}\ln K\int\frac{dx}{(2\pi)}f(x)\frac{x^4-3x^2}{(x^2+1)^3}.\end{aligned} \tag{3.8}$$

Although the latter expression is divergent in the limit $x \to \infty$, the sum,

$$\delta\left(\frac{1}{2m}\right) = \frac{1}{2mN}\ln K\int_{-\infty}^{\infty}\frac{dx}{2\pi}f(x)\frac{1-3x^2}{(1+x^2)^3}, \tag{3.9}$$

is convergent. Therefore the mass has a logarithmic dependence on cutoff, as expected. This enables us to write down the RG equations for the electron mass m,

$$\frac{d\ln m(\ell)}{d\ell} = -\frac{\alpha_1}{2N};\quad \ell \equiv \ln(K_0/K), \tag{3.10}$$

where

$$\alpha_1 \equiv \frac{1}{2\pi}\int dx\, f(x)(1-3x^2)/(1+x^2)^3 \approx -0.078. \tag{3.11}$$

Since $\alpha_1/(2N) < 10^{-2}$ is very small we shall neglect this mass renormalization for the rest of this analysis.

B. Renormalization of the contact interactions

We now consider the renormalization of the short-range interactions. Based on our assumption that the bare values $g_{\mathcal{A}}$ are small we will work to order g^2 and to lowest order in $1/N$.

The leading logarithmic corrections to the coupling constants of the contact interaction (2.10) are shown in Fig. 6(c). Straightforward calculation of those diagrams yield[35] the set of RG equations for the 8 coupling constants $g_{\mathcal{A}}$:

$$\frac{dg_{ij}}{d\ell} = -\frac{\alpha_3}{N^2}\delta(E_2)_{ij} - \frac{\alpha_1+2\alpha_2 A_{ij}}{N} g_{ij} - \sum_{kl}^{\sim} \frac{g_{kl}}{N}\alpha_2 B_{ij}^{kl} - 2N A_{ij} g_{ij}^2 + \sum_{kl}^{\sim}\sum_{mn}^{\sim} C_{klmn}^{ij} g_{kl} g_{mn}, \tag{3.12}$$

where

$$\begin{aligned} A_{ij} &\equiv -\frac{1}{16}\sum_{\gamma=x,y} \mathrm{tr}\left(\left[\hat{\tau}_i^{KK'}\hat{\tau}_j^{AB}, \hat{\tau}_z^{KK'}\hat{\tau}_\gamma^{AB}\right]^2\right), \quad B_{kl}^{ij} \equiv \frac{1}{64}\sum_{\gamma=x,y} \mathrm{tr}\left(\hat{\tau}_k^{KK'}\hat{\tau}_l^{AB}\left\{\hat{\tau}_i^{KK'}\hat{\tau}_j^{AB}, \hat{\tau}_z^{KK'}\hat{\tau}_\gamma^{AB}\right\}\right)^2, \\ C_{klmn}^{ij} &= \frac{1}{8}\sum_{\gamma=x,y} \mathrm{tr}\left(\hat{\tau}_k^{KK'}\hat{\tau}_l^{AB}\hat{\tau}_i^{KK'}\hat{\tau}_j^{AB}\hat{\tau}_z^{KK'}\hat{\tau}_\gamma^{AB}\left[\hat{\tau}_k^{KK'}\hat{\tau}_l^{AB}, \hat{\tau}_z^{KK'}\hat{\tau}_\gamma^{AB}\right]\hat{\tau}_i^{KK'}\hat{\tau}_j^{AB}\right) \\ &\quad + \frac{1}{64}\sum_{\gamma=x,y}\left\{\mathrm{tr}\left(\hat{\tau}_i^{KK'}\hat{\tau}_j^{AB}\left[\hat{\tau}_k^{KK'}\hat{\tau}_l^{AB}\hat{\tau}_z^{KK'}\hat{\tau}_\gamma^{AB}\hat{\tau}_m^{KK'}\hat{\tau}_n^{AB} + \hat{\tau}_k^{KK'}\hat{\tau}_l^{AB}\hat{\tau}_z^{KK'}\hat{\tau}_\gamma^{AB}\hat{\tau}_m^{KK'}\hat{\tau}_n^{AB}\right]\right)\right\}^2 \\ &\quad + \frac{1}{32}\left\{\mathrm{tr}\left(\hat{\tau}_i^{KK'}\hat{\tau}_j^{AB}\left[\hat{\tau}_k^{KK'}\hat{\tau}_l^{AB}, \hat{\tau}_m^{KK'}\hat{\tau}_n^{AB}\right]\right)\right\}^2. \end{aligned} \tag{3.13}$$

Here $\tilde{\sum}_{ij}$ is a sum over $i,j = \{0,x,y,z\}$ excluding the combination $i = 0, j = 0$ and the summation convention is not used. The symbol $\delta(E_2)_{ij}$ is 1 when $i = z$ and $j = x,y$ and 0 otherwise. By appearance there are 16 equations contained in Eq. (3.12). However several of these are identical due to the $\mathcal{D}_{3d}''$ symmetry so there are only eight independent equations for the flow of the eight independent coupling constants. The numerical coefficient α_1 is defined in Eq. (3.11) and

$$\alpha_2 \equiv \int \frac{dx}{2\pi}\frac{2f(x)}{(1+x^2)^2} \approx 0.469, \tag{3.14}$$

$$\alpha_3 \equiv \int \frac{dx}{2\pi}\frac{f(x)^2}{4(1+x^2)^2} \approx 0.066. \tag{3.15}$$

The term $2NA_{ij}g_{ij}^2$ in Eq. (3.12) corresponding to leading loop diagram (v) in Fig. 6(c) is naively the most significant quadratic term in Eq. (3.12), because it is leading in N. This term represents screening of repulsive interactions in the charge channel as expected in a fermionic system (since $A_{ij} \geqslant 0$). Note that this term is actually zero for the representation E_2'' and A_2, because these interactions commute with the single-particle Hamiltonian. Therefore, to lowest order in $1/N$, the interactions E_2'' and A_2 are unscreened and free to grow strongly attractive. We hasten to add that the higher order terms in Eq. (3.12) are very important and one cannot understand the behavior of the RG flows based only on the leading terms.

The single-particle Hamiltonian is off-diagonal so there is a contribution of order g^0N^{-2} to the coupling g_{E_2} from the two Coulomb line diagrams in Fig. 6(c) (iii), (iv). These may be calculated

$$\begin{aligned} &\int \frac{d^2k d\omega}{(2\pi)^3}\left[\frac{\pi f\left(\frac{2m\omega}{k^2}\right)}{Nm}\right]^2 \hat{G}(k,\omega)\otimes(\hat{G}(k,\omega)+\hat{G}(k,-\omega)) \\ &= 2\int \frac{d^2k d\omega}{(2\pi)^3}\left(\frac{\pi f\left(\frac{2m\omega}{k^2}\right)}{Nm}\right)^2\left(\frac{k^2}{2m}\right)^2 \\ &\quad\times\left(\frac{\tau_z^{KK'}\tau_+^{AB}\otimes\tau_z^{KK'}\tau AB_- + \mathrm{H.c.}}{\left[\omega^2+\left(\frac{k^2}{2m}\right)^2\right]^2}\right) \\ &= \frac{\pi}{N^2 m}\int\frac{dk}{k}\int\frac{dx}{2\pi}\frac{f(x)^2}{(1+x^2)}\sum_{\gamma=x,y}\left(\tau_z^{KK'}\tau_\gamma^{AB}\otimes\tau_z^{KK'}\tau_\gamma^{AB}\right) \\ &= \frac{4\pi\alpha_3}{N^2 m}\ln K\sum_{\gamma=x,y}\left(\tau_z^{KK'}\tau_\gamma^{AB}\otimes\tau_z^{KK'}\tau_\gamma^{AB}\right). \end{aligned} \tag{3.16}$$

From this, it follows the that the free field point $g_{\mathcal{A}} = 0$ is not a fixed point. Even if the the system starts with all bare couplings $g_{\mathcal{A}}(\gamma_1/2) = 0$ it will flow under RG to have finite g_{E_2} and g_{B_1} with the other couplings fixed to zero by the SU(4) symmetry of the single-particle Hamiltonian. To demonstrate the behavior in this regime we ignore momentarily g_{B_1} which gives us a single equation for g_{E_2},

$$\begin{aligned} \frac{dg_{E_2}(\ell)}{d\ell} &= -\frac{1}{N(N+2)}\left(\frac{\alpha_3(N+2)}{N} - \frac{(\alpha_2-\alpha_1)^2}{8N}\right) \\ &\quad - 2(N+2)\left(g_{E_2} - \frac{\alpha_2-\alpha_1}{4N(N+2)}\right)^2. \end{aligned} \tag{3.17}$$

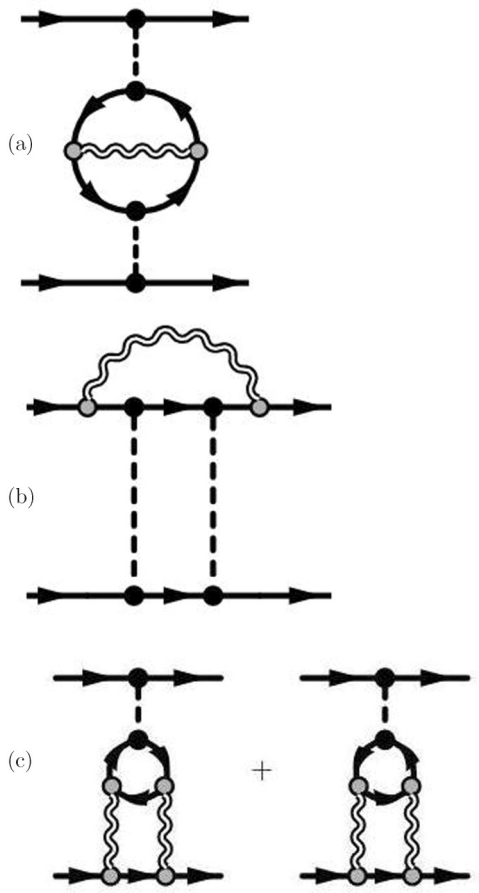

FIG. 7. (a) Schematic representation of the "bubble" diagrams where the shaded blob represents all possible connected diagrams, and arbitrary Coulomb propagators may be added. (b) Similar representation of the "ladder" diagrams. The leading diagrams from both of these groups are included, even though this is not strictly parametrically correct. (c) A second loop contribution to the anomalous dimension of the coupling g_{E_2} which is disregarded.

Since the first term on the right-hand side is negative, there can be no fixed point, and g_{E_2} flows to $-\infty$ regardless of the initial conditions. [This holds whether we treat Eq. (3.17) to lowest order in N or simply plug in $N = 4$.] According to the mean-field theory (see Sec. IV), this suggests a nematic ground state[35] with transition at $\approx$100 mK.

C. Applicability of our approximations

Let us turn to the justification of only including the diagrams in Fig. 6(c) in our treatment. Notice that it is different from the conventional $1/N$ approximation; see, e.g., Ref. 36. There are two issues: (1) There are two loop diagrams which are leading order in $1/N$ but are not included, Fig. 7(c); and (2) there are diagrams that are subleading in N which are taken into account [compare the bubble and ladder diagrams in Fig. 6(c)].

To address the first issue, let us discuss the diagrams of Fig. 7(c) in more detail. They are nonvanishing only for g_{E_2} and have the form $\delta g_{E_2} \sim \frac{g_{E_2}}{N}[C \ln^2(K) + D \ln(k)]$. The term $\ln^2$ is produced by two iterations of the RG equations [by substituting diagrams (iii) and (iv) in Fig. 6(c) into diagram (v)] but the second term does contribute to the linear term in the RG equation $2\alpha_2 A_{E_2} \to 2\alpha_2 A_{E_2} + D$. The constant D, however, depends on the cutoff scheme so that the term linear in g_{E_2} in the RG equation for g_{E_2} is not known (for the other constants it is well defined). Fortunately, is does not matter for the divergent behavior at large N. Consider the situation with all other constants except g_{E_2} fixed to zero, keeping only coefficients leading in $1/N$, compare Eq. (3.17),

$$\frac{dg_{E_2}}{d\ell} = -\frac{\alpha_3}{N^2} - \frac{\alpha_1 + 2\alpha_2}{N} g_{E_2} - 2N g_{E_2}^2. \qquad (3.18)$$

The quadratic term dominates the constant term when $g_{E_2} \geqslant N^{-3/2}$ at this point, but then the linear term is smaller by a factor of $1/\sqrt{N} \ll 1$. Thus, contrary to initial appearance, the linear term is of higher order in $1/N$ for g_{E_2}—so that we leave it in Eq. (3.12) only for simplicity. It makes essentially no difference to the evolution of the RG equations.

To address the second question we notice that the bubble diagram Fig. 6(c) (v) contains an extra factor of N in comparison with diagrams (vi), (vii), (viii). The latter diagrams are not diagonal in terms of the coupling constant, as given by the tensor C^{ij}_{klmn}, whereas the bubble diagram is $\propto N g^2_{ij}$ by construction. The large amounts of constants involved in the nondiagonal term may overcome the factor of N in the diagonal terms; therefore keeping both is legitimate. The higher order terms may be considered as $1/N$ corrections to the tensors A_{ij} and C^{ij}_{klmn}, respectively. For example, Fig. 7(a) is a leading $1/N$ correction to A_{ij}, whereas Fig. 7(b) is a leading $1/N$ correction to C^{ij}_{klmn}, even though the two diagrams do not have the same order in N.

Finally, we compare our treatment to the existing theoretical contributions. The first attempt at an RG treatment of BLG can be found in Ref. 11; however it does not appear consistent with our results.[37] The work of Vafek and Yang[14] is similar in spirit but contains only the G_1 and B_2 out of the eight possible representations and treats the Coulomb interaction as short range. The later work of Vafek[8] contains the RG equations for the full eight constants but again treats the Coulomb interaction as short ranged. The treatment of Ref. 3 is completely at the mean-field level and corresponds to counting only the diagrams from Fig. 6(c) marked (i) and (ii), which is not a parametrically justified approximation as well as considering only the B_2 representation. Reference 12 considered a mean-field theory of BLG; however their results appear to depend on an unrealistically strong next nearest neighbor interaction. Reference 38 attempted to calculate numerically the functional RG equation keeping the full momentum dependence of the four-fermion interaction and calculating the beta function perturbatively—this is not a parametrically justified treatment.

IV. RG FLOWS, THEIR TERMINATION, AND RENORMALIZED MEAN-FIELD TREATMENT OF SYMMETRY BREAKING

In this section we describe the numerical analysis of the coupling constant RG flows described by Eq. (3.12) and show that there are no weak-coupling fixed points. The divergence of coupling constants in 2D at zero temperature indicates spontaneous symmetry breaking. (Unlike in 1D the quantum

fluctuations in 2D are not infrared divergent and do not destroy zero-temperature phases.) We analyze the resulting phases within mean-field theory, using the coupling constants renormalized by the RG. This treatment is superior to simply doing mean field starting from the high energy scale since in that case the large logarithms are not summed in a controlled fashion.

A. General structure

If the initial RG conditions are such that $g_{\mathcal{A}}(\gamma_1/2) \neq 0$, then the SU(4) symmetry is absent and we must consider the flow of all the coupling under the RG. Determining whether there exist any fixed points cannot be done analytically as it requires solving a polynomial of the 64th order. However, a numerical solution shows that there exist no fixed points. Therefore at least some of the couplings must grow infinitely. At the same time, the leading term quadratic in the couplings in Eq. (3.12) $\sim N g^2$, always with a nonpositive coefficient, so we expect generically that large positive coupling will be driven back to zero. For all positive initial coupling constants, this means that the system will be driven to the free field point until g_{E_2} becomes large and negative. This behavior is confirmed by the numerical evolution of the RG equations (see Fig. 8 where g_{E_2} always becomes negative and increases until the other couplings diverge).

Note that although we have set the current-current couplings g_{B_1}, g_{A_2}, g_{E_1}, and $g_{E_1''}$ to zero initially, they are generated through renormalization. The examples of the RG equation shown in Fig. 8 indicate the current-current couplings become of the same order as the density-density couplings at low energies. Therefore we cannot ignore the current-current interactions when analyzing the ground state, and ignoring them would lead to misleading results.

The coupling g_{B_2} has been given special emphasis in some of the earlier studies.[5] We find that in the RG equations it does not seem to play an exclusive role, as can be seen in Fig. 9, where it is screened efficiently—the leading term in the RG flow is $2N g_{B_2}^2$. Note that large positive initial g_{B_2} does not provoke a phase transition to the AF state on its own (see Fig. 8). Once g_{E_2} becomes relatively large the presence of a finite g_{B_2} will change the structure of the flow, especially since it breaks the SU(4), however not in a marked way. For example, starting with all other couplings set to zero except for g_{B_2}, g_{E_2} still becomes the most significant negative coupling, and the nematic phase is the preferred phase. As a result, g_{B_2} is perhaps the least important of the four couplings. This is not a conclusion that can be reached on general grounds, but only by solving the detailed RG equations over a broad range of parameters. Moreover, at least some of the couplings behave nonmonotonically. Initially negligible coefficients may end up diverging quickly [e.g., g_{A_2} in Fig. 8(a)]. At the same time a coupling that is not large at the end of the RG flow may change the character of the flow in the initial stages.

The RG equations contain terms up to second order in g. Therefore, it may be easily seen that since there is no fixed point, the couplings always go to infinity as $g_{\mathcal{A}} \sim \lambda_{\mathcal{A}}(\ell_0 - \ell)^{-1}$ where ℓ_0 gives the value of the singularity in the RG flow and the $\lambda_{\mathcal{A}}$ determine how quickly each constant

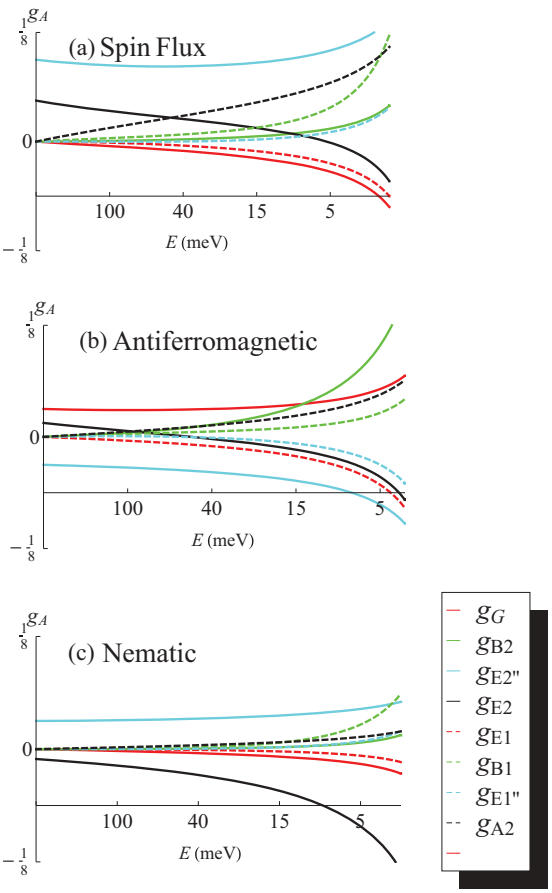

FIG. 8. (Color online) Plots of the coupling constant as a function the running RG scale $\ell = \ln(K_0/K)$. There are eight running couplings labeled by the corresponding representation. The density-density couplings are given by solid lines, the current-current couplings by dashed. The graphs end when the couplings become of order $1/N = 1/4$. They reach a singularity a finite ℓ soon after the graph ends.

diverges. Mathematically, there are six sets of $\{\lambda_{\mathcal{A}}\}$ that satisfy the RG equations and are stable to perturbation. One might be tempted to determine the ground state, using this mathematical feature, via the coefficients $\lambda_{\mathcal{A}}$. However these coefficients are meaningful only for the RG at $g_{\mathcal{A}} \gg 1$ which is outside the range of validity of the proposed theory and the RG equation (3.12). Moreover, $g \to \infty$, indicates an instability towards a broken symmetry states, so that we shall use a mean-field theory starting from the energy scale where some of the couplings become sufficiently large.

B. Ground-state energies within renormalized mean-field approach

The unbounded growth of coupling constants in the RG flow generally indicates the development of a spontaneous symmetry breaking and the opening of a gap. To describe the corresponding phase transition we use a self-consistent mean-field theory. The self-consistent mean-field theory is implemented by replacing all possible pairs of fermions in the quartic interaction terms with their mean values. For this we introduce the Gorkov-Nambu vectors which adjoin the two

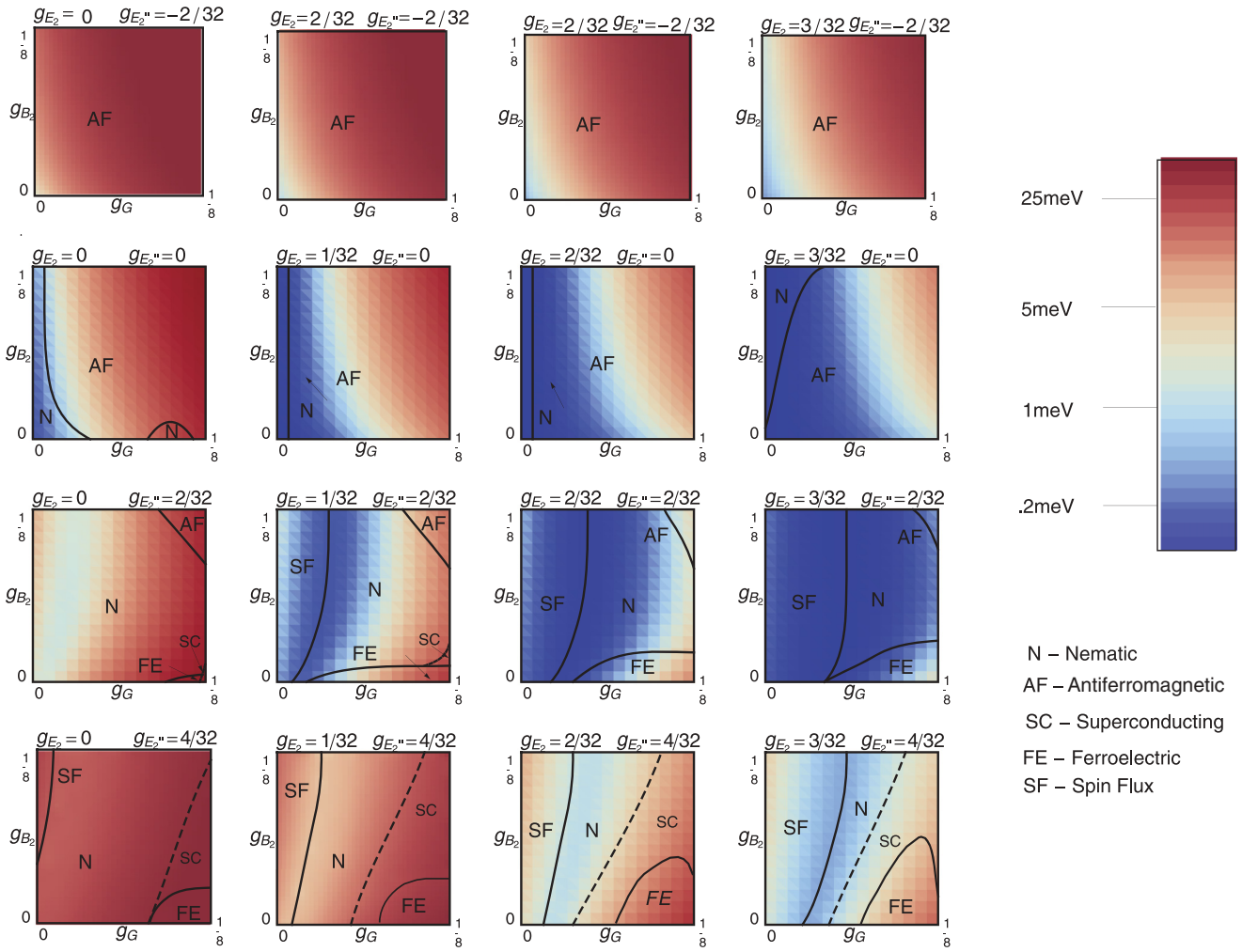

FIG. 9. (Color online) Plot of the broken symmetry phase and energy scale for BLG as a function of bare coupling constants. When the energy scale is less than $E_{\mathrm{LiTr}} \approx 1$ meV the broken symmetry state is in competition with the Lifshitz transition and the BLG may remain metallic (with eight Dirac points). Dashed line indicates the region where the triplet superconducting phase (SC) is very close in energy (but slightly above) to normal (nematic or ferroelectric) states.

8-component vectors ψ and $\psi^\dagger$ as follows,

$$\Psi(\boldsymbol{k}) \equiv \begin{pmatrix} \psi(\boldsymbol{k}) \\ \hat{\mathcal{T}}(\psi^\dagger(-\boldsymbol{k}))^t \end{pmatrix}_N, \qquad \Psi^\dagger(\boldsymbol{k}) \equiv (\psi^\dagger(\boldsymbol{k}), -[\psi(-\boldsymbol{k})]^t \hat{\mathcal{T}})_N, \tag{4.1}$$

where $\hat{\mathcal{T}} \equiv i\tau_y^{KK'}\tau_y^{AB}\sigma_y$ is the time reversal matrix. We also introduce Pauli matrices $\tau^N_{0,x,y,z}$ acting on the Nambu space. The vectors $\Psi^\dagger$ and Ψ satisfy the condition

$$\Psi^\dagger(\boldsymbol{k}) = i\Psi^t(-\boldsymbol{k})\tau_y^N\hat{\mathcal{T}}. \tag{4.2}$$

We rewrite the interaction terms with the help of the Nambu vectors

$$\sum_{ij}\left(\psi^\dagger\tau_i^{KK''}\tau_j^{AB}\psi\right)^2 = \frac{1}{4}\sum_s g_s(\Psi^\dagger\cdot\hat{M}_s\cdot\Psi)^2. \tag{4.3}$$

Here $M_s \equiv \tau_i^{KK'}\tau_j^{AB}\tau_k^N\sigma_l$ acts on the 16-dimensional space spanned by the Nambu vectors and we write s as a shorthand for the list $(ijkl)$. The couplings g_s are defined as $g_{abz0} = g_{ab}$, $g_{00z0} = g_{00}$, $g_{a000} = g_{a0}$, and $g_{0b00} = g_{0b}$, where $a,b = x,y,z$ and all other constants are zero. The factors of τ_z^N are necessary since we must have

$$\left(i\tau_y^N\mathcal{T}\right)M_s^t\left(i\tau_y^N\mathcal{T}\right) = -M_s \tag{4.4}$$

to satisfy both Eq. (4.2) and fermion anticommutivity.

The mean-field approximation consists of replacing pairs of fermionic operators in Eq. (4.3) with their expectation values as follows:

$$\begin{aligned}\frac{1}{4}\sum_s g_s(\Psi^\dagger\cdot\hat{M}^s\cdot\Psi)^2 &\approx \frac{1}{2}\sum_s g_s\Big\{\Psi^\dagger\cdot\hat{M}^s\cdot\Psi\langle\Psi^\dagger\cdot\hat{M}^s\cdot\Psi\rangle \\ &+ 2\Psi^\dagger\cdot(\hat{M}_s\cdot\langle\Psi\otimes\Psi^\dagger\rangle\cdot\hat{M}_s)\Psi - \frac{1}{2}(\langle\Psi^\dagger\cdot\hat{M}^s\cdot\Psi\rangle)^2 \\ &+ \mathrm{tr}[(\langle\Psi\otimes\Psi^\dagger\rangle\cdot\hat{M}_s)^2]\Big\}.\end{aligned} \tag{4.5}$$

Here we have used the fact that, according to Eqs. (4.2) and (4.4),

$$\Psi^\dagger\cdot\hat{M}^s\cdot\Psi=\Psi^t\cdot(i\tau_y\mathcal{T})\hat{M}_s^t(i\tau_y\mathcal{T})\cdot(\Psi^\dagger)^t=-\Psi^t\cdot\hat{M}^s\cdot(\Psi^\dagger)^t$$

to combine the Cooper and Fock terms.

Now we assume that the there is some nonzero expectation value of the fields which corresponds to a nonzero order in one of the phases classified in the Appendix.

$$\langle\Psi\otimes\Psi^\dagger\rangle\equiv-\frac{1}{2Nc_{\mathcal{A}}}\left(\frac{m}{4\pi}\right)\sum_\alpha\hat{M}^\alpha_{\mathcal{A}}\Delta^\alpha_{\mathcal{A}},\tag{4.6}$$

where matrices $\hat{M}^\alpha_{\mathcal{A}}$ are specified for each phase $\mathcal{A}$ in the Appendix and $\Delta_{\mathcal{A}}=\{\Delta^\alpha_{\mathcal{A}}\}$ is the order parameter, which is singlet or multicomponent depending on the phase. Below we will use the notation $|\Delta_{\mathcal{A}}|^2\equiv\sum_\alpha|\Delta^\alpha_{\mathcal{A}}|^2$. The effective interaction constant $c_{\mathcal{A}}$ is defined for each phase as,

$$c_{\mathcal{A}}\equiv\sum_s g_s\left\{\delta_{s\mathcal{A}}-\frac{1}{4N^2}\mathrm{tr}[(\hat{M}_s\hat{M}_{\mathcal{A}})^2]\right\}.\tag{4.7}$$

The assumption of a finite expectation value is consistent only if $c_{\mathcal{A}}<0$. The interaction mean-field energy is therefore

$$H_{sr}=\frac{1}{2}\sum_\alpha\Delta^\alpha_{\mathcal{A}}\left(\Psi^\dagger\cdot\hat{M}^\alpha_{\mathcal{A}}\cdot\Psi\right)-\frac{m}{8\pi c_{\mathcal{A}}}|\Delta_{\mathcal{A}}|^2.\tag{4.8}$$

Including the effect of the single-particle Hamiltonian $\hat{H}_0$, defined in Eq. (2.5), the total mean-field Hamiltonian is

$$H_{\mathrm{MF}}=\frac{1}{2}\sum_k\Psi^\dagger(\boldsymbol{k})\left[\hat{H}_0\tau_z^N+\sum_\alpha\Delta^\alpha_{\mathcal{A}}\hat{M}^\alpha_{\mathcal{A}}\right]\Psi(\boldsymbol{k})-\frac{m|\Delta_{\mathcal{A}}|^2}{8\pi c_{\mathcal{A}}},\tag{4.9}$$

for fixed values of the order parameters $\Delta^\alpha_{\mathcal{A}}$.

In the spirit of the Hartree-Fock or BCS theory, we diagonalize Eq. (4.9) to obtain the ground-state energy per unit area,

$$E_{\mathrm{MF}}(\{\Delta_{\mathcal{A}}\})=-N\int_{\frac{k^2}{2m}<\mathcal{E}_c}\frac{d^2k}{2\pi}\varepsilon(k,\Delta_{\mathcal{A}})-\frac{m|\Delta_{\mathcal{A}}|^2}{8\pi c_{\mathcal{A}}(\mathcal{E}_c)}.\tag{4.10}$$

Here $\varepsilon(k,\{\Delta_{\mathcal{A}}\})$ are the positive eigenvalues of the matrix $\hat{H}_0\tau_z^N+\sum_\alpha\Delta^\alpha_{\mathcal{A}}\hat{M}^\alpha_{\mathcal{A}}$ and the factor of N comes from the degeneracy. The energy scale $\mathcal{E}_c$ is the energy scale at which we stop the RG. The integral in Eq. (4.10) evaluates to

$$\int_{\frac{k^2}{2m}<\mathcal{E}_c}\cdots=\mathrm{const}+\frac{m|\Delta_{\mathcal{A}}|^2}{2\pi}\left(\alpha_{\mathcal{A}}+\beta_{\mathcal{A}}\ln\frac{\mathcal{E}_c^2}{|\Delta_{\mathcal{A}}|^2}\right),\tag{4.11}$$

where $\alpha_{\mathcal{A}}$ and $\beta_{\mathcal{A}}$ are coefficients that depend on the phase $\mathcal{A}$. The coefficients $\alpha_{\mathcal{A}}$ may be explicitly calculated from Eq. (4.10) (the value of $\beta_{\mathcal{A}}$ is irrelevant as we will see). We list here $\alpha_{\mathcal{A}}$ for the states where $\Delta\cdot M$ may be written as $\sum_{ijkl}u_iv_jw_kx_l\tau_i^{AB}\tau_j^{KK'}\sigma_k\tau_l^N$. Because of the symmetry of H_0 there are only three independent coefficients. Labeling the coefficient α by the representation and using the superscript n or s to denote normal or superconducting we have

$$\begin{aligned}&\alpha^n_{A_1}=\alpha^n_{A_2}=\alpha^n_{E_2''}=\alpha^s_{B_1}=\alpha^s_{B_2}=\alpha^s_{E_1''}=1,\\&\alpha^n_{B_1}=\alpha^n_{B_2}=\alpha^n_{E_1''}=\alpha^s_{A_1}=\alpha^s_{A_2}=\alpha^s_{E_2''}=\tfrac{1}{2}+\ln 2\approx 1.19,\\&\alpha^n_{E_2}=\alpha^n_{E_1}=\alpha^n_G=\alpha^s_{E_2}=\alpha^s_{E_1}=\alpha^s_G=\tfrac{1}{4}+\ln 2\approx 0.94.\end{aligned}\tag{4.12}$$

The coefficients for the spin singlet and spin triplet normal states are the same because of symmetry. These coefficients are sufficiently close to 1 that we have simply taken $\alpha_{\mathcal{A}}\approx 1$. the term $\beta_{\mathcal{A}}\ln\frac{\mathcal{E}_c^2}{\Delta^2}$ in Eq. (4.11) should be interpreted as the continuation of the RG flow from the scale $\mathcal{E}_c$ down to the energy $|\Delta|$. Although obtained by using mean-field theory, since the flow of $c_{\mathcal{A}}$ is governed by the RG equation (3.12), we have to replace the logarithmic correction to Eq. (4.11) with the evaluation of $c_{\mathcal{A}}$ at the energy Δ. The mean-field energy density is therefore written as

$$E(\Delta_{\mathcal{A}})=\frac{m}{8\pi}\left[-2N-\frac{1}{c_{\mathcal{A}}(|\Delta_{\mathcal{A}}|)}\right]|\Delta_{\mathcal{A}}|^2,\quad c_{\mathcal{A}}<0.\tag{4.13}$$

The ground state may now be determined by minimizing Eq. (4.13) with respect to $\Delta_{\mathcal{A}}$ with the $c_{\mathcal{A}}(\Delta)$ obtained by numerical integration of the RG equations. The ground-state energy gap will then be equal to the value of $|\Delta|$ at the minimum.

It is important to note that we expect to find this minimum when the coefficient $c(|\Delta|)\sim\frac{1}{2N}$ which is inside the range of validity for our RG equation, $g\sim 1/N$. The remaining subtlety is the inclusion of the long-range Coulomb interaction into the mean-field description. Usually, it enters in the statically screened limit $g_{00z0}\simeq 1/N$ and does not diverge at the transition. Furthermore, according to Eq. (4.7), this constant can produce only finite $1/N^2$ correction (positive to all superconducting states and negative for all normal states). Therefore, we will neglect g_{00z0} in the further manipulations.

V. THE PHASE DIAGRAM

The result of minimizing Eq. (4.13) is presented in Fig. 9. We find by extensive numerical investigation only five out of the possible sixty-four phases enumerated in the Appendix (10 in the charge channel, 22 in the spin channel, and 32 in the Cooper channel). They are the nematic phase, the antiferromagnetic phase, the spin-flux phase, and in the corners of the parameter space of bare interaction, ferroelectric phase, and singlet and triplet superconductor phases.

Note that it is also possible that the resulting gaps are smaller than the energy of the Lifshitz transition,[13] $\mathcal{E}_{\mathrm{LiTr}}\approx$ 1 meV. In this case the renormalization of coupling constants is stopped at $\mathcal{E}_{\mathrm{LiTr}}$, spontaneous symmetry breaking does not occur, and the system remains in the symmetric state with the four Dirac cone spectrum.

Figure 9 shows the results of the RG analysis in terms of the resulting symmetry broken phases. We find that there is significant variation in the scale $\mathcal{E}$, $\ln(\mathcal{E}_0/\mathcal{E})\sim 1\div 20$, as expected from the wide range of couplings analyzed. If we consider small initial couplings the $g_{\mathcal{A}}\ll 1/N$ then the RG is driven by the constant term and $\ln(\mathcal{E}_0/\mathcal{E})\sim 10$ irrespective of the initial conditions, resulting in a symmetry breaking only at extremely small energy scale $\mathcal{E}\sim 10^{-2}$ meV.

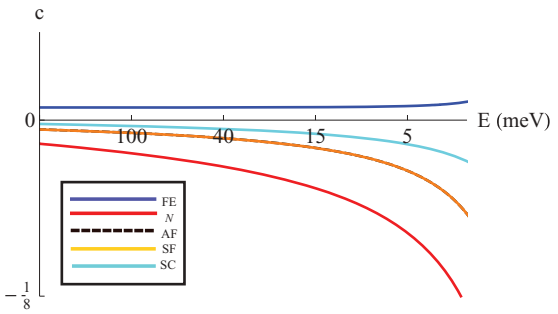

FIG. 10. (Color online) Interaction energy as a function of energy scale for selected phase with initial conditions $g_G = -0.0$, $g_{B_2} = 0.06$, $g_{E_2''} = 0$, $g_{E_2} = -0.03$, and all others zero. For these initial conditions the nematic phase is the ground state.

There is a variety of phases that have been proposed as the ground state of BLG that we do not find. A quantum anomalous Hall state (QAH) state was suggested in Ref. 9, corresponding to the representation g_{A_2} with order parameter $\langle\psi^\dagger\tau_z^{AB}\psi\rangle$. This is not found as a ground state in our analysis. In the same paper, and in Refs. 6 and 11, a large manifold of quantum Hall ferromagnetic states were suggested containing the representations E_2'', A_2, and B_2 in both spin singlet and spin triplet representation. All of these states were considered as degenerate appealing to the SU(4) symmetry of the single-particle Hamiltonian, Eq. (2.5). In both cases the artificial SU(4) symmetry was assumed to be exact, which is contradicted by the importance of the short-range interactions we find here in solving the complete set of RG equations. The loop current state of Ref. 12 corresponding to representation A_2 in the singlet channel also does not appear. In Ref. 38 they suggest a "CDW$_3$ state," which is in the singlet G representation. We do not find it here.

In the subsections below, we discuss the details of each phase. We will present comparative flows of the couplings defined in Eq. (4.7) to illustrate the competition between phases; see Figs. 10–15.

A. Nematic phase (N)

In the nematic phase, there is a finite expectation value for the order parameter $\langle\psi^\dagger\tau_z^{KK'}\tau_{x,y}^{AB}\psi\rangle$, breaking the rotational symmetry of the system from sixfold to twofold while

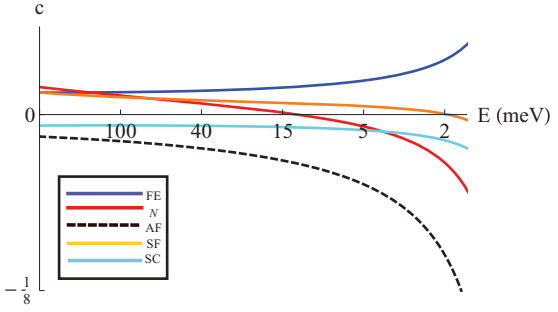

FIG. 11. (Color online) The interaction energy as a function of energy scale for some choice of initial parameters with initial conditions $g_G = -0.075$, $g_{B_2} = 0.06$, $g_{E_2''} = 0$, $g_{E_2} = 0.015$, and all others zero. In this case the ground state is the AF phase.

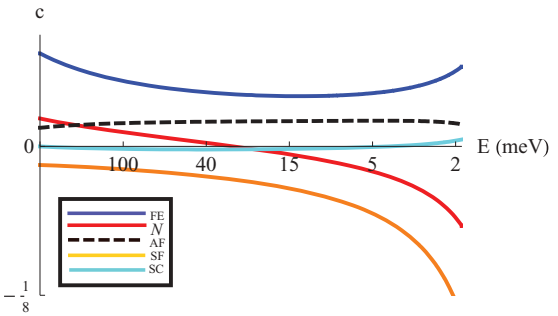

FIG. 12. (Color online) Interaction energy for selected phases a function of energy scale with initial conditions $g_G = 0$, $g_{B_2} = 0.06$, $g_{E_2''} = 0.06$, $g_{E_2} = 0.03$, and all others zero. In this case the ground state is the spin flux state shown in orange.

maintaining translational symmetry. The order parameter is characterized by enhanced electron hopping in one direction. The interaction energy for this phase depends on the combination of parameters obtained from Eq. (4.7):

$$c_N = \tfrac{1}{8}g_{B_2} - \tfrac{1}{4}g_{E_2''} + g_{E_2} + \tfrac{1}{8}g_{B_1} - \tfrac{1}{8}g_{E_1''} - \tfrac{1}{8}g_{A_2}. \quad (5.1)$$

It is the preferred ground state in the absence of intervalley scattering, and it is also generally the ground state when the bare g_{E_2} coupling is negative. Note that a negative contribution towards bare g_{E_2} comes from the electron-electron interaction via the polarization of the lattice, i.e., via virtual excitation/absorption of in-plane phonons near the Γ point. The nematic phase is also the ground state over other large parts of the parameter space as can be seen in Fig. 9. This reflects the fact that the coupling g_{E_2} almost always becomes negative rapidly (see Fig. 8).

We previously proposed the nematic phase as a possible ground state based on a more limited analysis of the RG equations.[13] Using a similar renormalization group analysis Vafek and Yang[8,14] also find the nematic phase as a possible ground state, supporting the analysis in this paper.

The most notable characteristic of the nematic phase is that it remains gapless, but with the parabolic bands reconstructed into two Dirac minicones at energies less than $|\Delta|$. The nematic phase would show metallic behavior in conductance

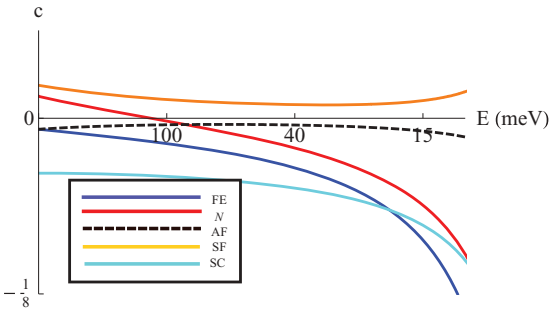

FIG. 13. (Color online) The evolution of the interaction energy of the selected phases as a function of the energy scale with initial conditions $g_G = 0.06$, $g_{B_2} = 0$, $g_{E_2''} = 0.06$, $g_{E_2} = 0.075$, and all others zero. In this case the ground state is a ferroelectric phase. The difference in energy between the F phase and nearby phases is quite small.

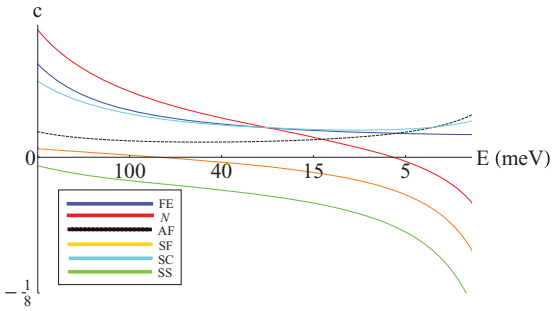

FIG. 14. (Color online) Interaction energy for selected phases as a function of the energy scale with initial conditions $g_G = -0.045$, $g_{B_2} = 0.06$, $g_{E_2''} = -0.06$, $g_{E_2} = 0.09$, and all others zero. In this case the singlet superconducting phase is the ground phase.

measurements, but decreasing density of states at low densities. The nematic state preserves time reversal symmetry and so it should not show asymmetry between positive and negative magnetic fields in magneto-transport. The nematic order parameter transforms in the same representation of $\mathcal{D}_{3d''}$ as uniaxial strain so that strain will couple directly to this state. It is possible that strain could induce a transition into the nematic phase,[39] even if unperturbed BLG chooses another phase as the ground state.

B. Antiferromagnetic phase (AF)

The antiferromagnetic phase is defined by a nonzero expectation value of $\langle \psi^\dagger \tau_z^{AB} \tau_z^{KK'} \vec{\sigma} \psi \rangle$. This state corresponds to opposing magnetic moments on the A and B sublattices. The orbital part breaks the reflection symmetry between the two sublattices but otherwise preserves the $\mathcal{D}_{3d}''$ symmetry of the BLG in its entirety.

The exchange energy depends on the following combination of coupling constants obtained from Eq. (4.7):

$$c_{AF} = -\tfrac{1}{2} g_G - \tfrac{1}{8} g_{B_2} + \tfrac{1}{4}(g_{E_2''} + 2g_{E_2} + g_{E_1} + g_{E_1''}) - \tfrac{1}{8} g_{B_1} - \tfrac{1}{8} g_{A_2}. \quad (5.2)$$

The AF is promoted strongly by the coupling g_G, with the factor of 4 coming from the dimension of the representation G.

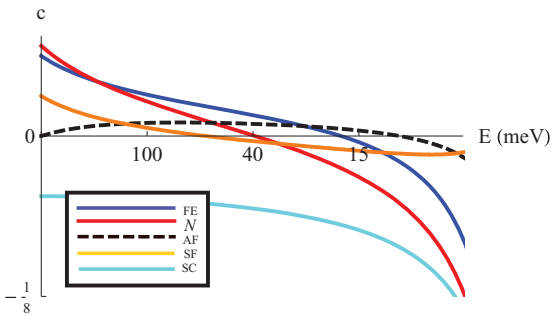

FIG. 15. (Color online) Interaction energy for selected phases as a function of the energy scale for initial repulsive short-range interaction. In this case the triplet superconducting phase is very close to the ground phase with initial conditions $g_G = 0.06$, $g_{B_2} = 0.06$, $g_{E_2''} = -0.12$, $g_{E_2} = 0.06$, and all others zero. Even though c_{SC} appears to be the most negative, minimization of Eq. (4.13) gives the nematic state as a preferred ground state.

This effect is amplified by the sensitivity of the RG equations to the coupling g_G. As a result even small values of g_G near the free field point make the AF state the ground state. The AF state is also promoted by negative $g_{E_2''}$ and is generally the ground state when we start with negative $g_{E_2''}$. Again we emphasize that these conclusions come from the combination of RG equations and interaction energy, not just from the interaction energy alone. Other authors have proposed this AF state as a possible ground state. Kharitonov[5] suggested the AF state based on experimental evidence and simple mean-field theory arguments applied at the high-energy scale directly. The structure of our RG equations indicates that such a simple mean-field theory is not applicable to BLG, although it does suggest the same state.

The AF phase is expected to be an insulating state with activated gap behavior in transport measurements. Although the magnetic field does not couple directly to the AF state since it is antiferromagnetic, the Zeeman energy splitting does break the SU(2) spin symmetry of the system (spin-orbit is negligible). The LAF state is adiabatically connected to a quantum Hall ferromagnetic state at higher magnetic field. A lack of features between the zero and high magnetic field state might be the evidence that the zero magnetic field state is AF.[5]

C. Spin-flux (spin-Hall) phase (SF)

The spin-flux (SF) phase (elsewhere called a quantum spin Hall state) is defined by the finite expectation value of $\langle \psi^\dagger \tau_z^{AB} \vec{\sigma} \psi \rangle$. The effect of this on the electrons is equivalent to the development of a finite spin-orbit coupling, and gaps the electronic spectrum. It may be viewed as a state where spin currents circle the honeycomb rings, or as a quantum anomalous Hall effect state, but with opposite signs for opposite spins, producing no net charge current, so that this state preserves time reversal invariance.

The interaction energy of the SF depends on the combination of coupling constants obtained from Eq. (4.7):

$$c_{SF} = \tfrac{1}{4}(g_{E_2''} - g_{E_2} + g_{E_1} - g_{E_1''}) - \tfrac{1}{8}(g_{B_2} + g_{B_1} + g_{A_2}). \quad (5.3)$$

The SF state has a similar matrix structure as the AF state and therefore a similar interaction energy. However it is not promoted by large g_G, unlike the AF phase. Therefore, generically, large g_G generally suppresses the SF in favor of other states as can be seen in Fig. 9.

Analogously to the case of spin-orbit coupling in monolayer graphene,[40] the finite value of the spin-flux order parameter may create a "spin Hall effect" with quantized spin-Hall conducivity. The edge states and insulating bulk imply a quantized conductance of $4e^2/h$, unless they are localized by magnetic and intervalley-scattering disorder. The state is time reversal invariant, so no transverse conductance at zero magnetic field is possible.

D. At the limits of applicability: Ferroelectric phase

The ferroelectric (FE) phase is characterized by a nonzero expectation value of $\langle \psi^\dagger \tau_z^{AB} \tau_z^{KK'} \psi \rangle$. It is a spontaneous charging of the BLG with opposite charge on the two layers.

The interaction energy for this phase depends on the combination of couplings obtained from Eq. (4.7):

$$c_F = \tfrac{7}{8}g_{B_2} + \tfrac{1}{4}(g_{E_2''} - g_{E_2} + g_{E_1} - g_{E_1''}) - \tfrac{1}{8}g_{B_1} - \tfrac{1}{8}g_{A_2}. \tag{5.4}$$

We find that the ferroelectric phase is strongly suppressed by positive bare g_{B_2} and the development of the FE phase requires the g_{B_2} coupling to diverge to negative infinity, which can only happen in a small sliver of the phase space where the combination of the higher order diagrams conspire to drive g_{B_2} negative. Even in this section the energy difference between the ferroelectric and competing phases is never large, and it may be that in a more accurate calculation it never appears as the ground state.

The FE state was also proposed in Ref. 3. However this analysis was based on a flawed mean-field theory treatment counting only the diagrams from Fig. 6(c) marked (i) and (ii) as well as considering only the single-parameter scaling theory with one interaction constant in the B_2 channel. These are not parametrically justified approximations.

The ferroelectric phase is a completely gapped state, with neither neutral nor charged excitations. It is also a trivial insulator in that it does not possess protected edge modes. Therefore, it should display insulating transport behavior. An external field perpendicular to the BLG flake would promote the FE phase, increasing the gap due to the interlayer symmetry breaking at the single-particle level.[1] This does not seem to take place in any of the recent experiments[16,18] on BLG, where the external transverse field destroyed the zero-field state, and introduced a distinct state determined by the interlayer asymmetry.

E. At the limits of applicability: Superconducting phases

The singlet superconducting (SS) phase is characterized by the usual order parameter $\langle\psi^\dagger\mathcal{T}\psi^\dagger\rangle$. The coupling for this phase is found from Eq. (4.7) to be

$$c_{SS} = \tfrac{1}{2}g_G + \tfrac{1}{8}g_{B_2} + \tfrac{1}{4}(g_{E_2} + g_{E_2''} - g_{E_1} - g_{E_1''}) - \tfrac{1}{8}g_{A_2} - \tfrac{1}{8}g_{B_1}. \tag{5.5}$$

The stability of this phase requires very significant negative couplings from the very beginning and the phase cannot arise from the purely repulsive interaction.

The triplet superconducting (SC) phase has the order parameter $\langle\psi^\dagger\tau_z^{KK'}\vec{\sigma}\mathcal{T}\psi^\dagger\rangle$, with the pairing function of the opposite signs in the K and K' valleys. Its interaction depends on the combination of couplings obtained from Eq. (4.7):

$$c_{SC} = -\tfrac{1}{2}g_G + \tfrac{1}{8}g_{B_2} + \tfrac{1}{4}(g_{E_2} - g_{E_2''} - g_{E_1} + g_{E_1''}) - \tfrac{1}{8}g_{A_2} - \tfrac{1}{8}g_{B_1}. \tag{5.6}$$

For the repulsive interaction, the triplet SC phase only appears as a stable phase at large couplings.

To conclude, both superconducting phases appear only on the limits of the applicability of the theory. Moreover, finite values of the underscreened Coulomb interaction push the energies of those stated farther up. It is therefore possible that the appearance of the SC phases is merely an artifact of our inability to deal properly with strong couplings, and that the superconductivity does not belong to the actual phase diagram.

VI. CONCLUSION

Several results have been established in this paper. The ground state of BLG cannot be understood without considering the high-energy couplings in detail, because different couplings lead to different ground states. Moreover naive expectations about the importance of certain couplings are not borne out and all plausible combinations must be considered. In particular excluding intervalley scattering leads to misleading results. The previously reported nematic state is the ground state for a significant fraction of these couplings. Of the large number of ground states that are possible we find that only five appear. They are nematic, antiferromagnetic, ferroelectric, and triplet superconductor, as well as a "spin-flux" phase not previously proposed. The nematic, antiferromagnetic, and spin-flux phases seem the most likely candidates.

The present work may be extended in a variety of ways. The accuracy of the renormalization group equations may be improved and validated by considering higher order diagrams and a more detailed mean-field theory constructed. One may also try to connect the value of the couplings at the scale $\gamma_1/2 \approx 0.2$ eV with their value at the bandwidth of the π orbitals. The possible phase transitions between the proposed states and the behavior of domain walls between regions of different phases may be needed to properly account for the transport data.

Such improvements aside, the unique challenge of theoretically determining the electronic ground state of BLG has been laid out. The problem naturally involves the competition of an uncommonly large set of phases and interactions. Truncating the theory to a more tractable subset does not appear to give accurate results. Instead the problem must be attacked in its full complexity.

ACKNOWLEDGMENTS

This work was supported by an ERC Advanced Investigator Grant, EPSRC Grant No. EP/G041954, and the Royal Society. Also, the authors thank M. Kharitonov for reading the manuscript, M. Mucha-Kruczynski for technical assistance, and the KITP-UCSB research program "The Physics of Graphene" for hospitality during the final stage of this work.

APPENDIX: GROUP THEORY FOR PHASES IN BLG

In this Appendix we classify the possible phases of BLG. We will use the matrix notation defined in Sec. II.

Phases are defined by all possible expectations $\Delta \equiv \langle\Psi \otimes \Psi^\dagger\rangle$ that belong to an irreducible representations (irrep) of the symmetry group $\mathcal{G}$ of BLG. Every phase defines a subgroup $\mathcal{H}$ of $\mathcal{G}$ consisting of all operations that leave Δ invariant. Two phases within an irrep are distinct if their invariant subgroups are not conjugate. (Recall that two subgroups $\mathcal{H}$ and $\mathcal{H}'$ of a group $\mathcal{G}$ are conjugate if they are an element of $g \in \mathcal{G}$ such that $g\mathcal{H}g^{-1} = \mathcal{H}'$.) This definition is correct in the sense that it gives all physically distinct states that may be reached via a second-order phase transition at the highest critical temperature, per the usual Landau theory.

Let us notice, however, that the anomalous averages belonging to the same irrep of the original group $\mathcal{G}$ may correspond to the different phases. For example, $\Delta_I = \tau_y^{AB}\tau_y^{KK'}$ and $\Delta_{II} = \tau_x^{AB}\tau_x^{KK'} + \tau_y^{AB}\tau_y^{KK'}$ are both charge density waves

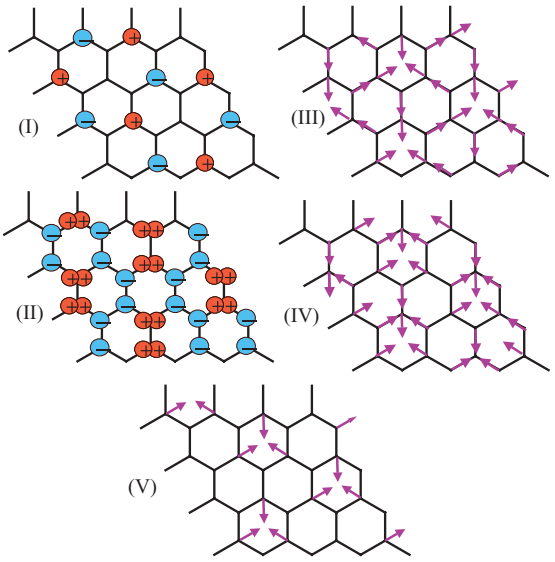

FIG. 16. (Color online) Sketch of the symmetric magnetic and normal phases transforming according the G representation. (I) G_1 normal state; (II) G_2 normal state; (III) G_3 spin state; (IV) G_4 spin state; (V) G_5 spin state. Because of the absence of spin-orbit coupling the overall direction of the spins is arbitrary.

with a tripled unit cell transforming in the G representation. However, these two phases are distinct since Δ_{II} is invariant under rotations by $2\pi/3$ around a lattice site, whereas Δ_I is not invariant under any conjugate operation; see Fig. 16. As a further example, a canted antiferromagnetic phase would be given by $\Delta = \tau_x^{AB}\tau_z^{KK'}\sigma_x + \sigma_z$. This is not considered in the present classification since it does not belong to an irrep of $\mathcal{G}$ (it is a linear combination element of the B_2 and A_1 representations). Of course all such mixed states may be constructed from linear combinations of phases in our classification.

We classify the phases according to the symmetry group $\mathcal{G}$ of BLG which is effective at intermediate energies; see Sec. II. In this regime the effect of RG irrelevant perturbations such as umklapp scattering may be ignored, and RG relevant but weak perturbations, such as trigonal warping and spin-orbit coupling, may be neglected. This approximation should be effective at energies between $\gamma_1/2 = 0.2$ eV and $\mathcal{E}_{\mathrm{LiTr}} = 1$ meV, which contains any energy scale associated with spontaneous symmetry breaking. In this regime the symmetry group is

$$\mathcal{G} = \mathcal{D}_{\mathrm{inf}}^{(\mathrm{rot})} \times \mathcal{D}_{\mathrm{inf}}^{(\mathrm{tran})} \times \mathrm{SU}(2)^{(\mathrm{spin})} \times U(1)^{(\mathrm{gauge})} \times T. \quad \text{(A1)}$$

The first subgroup, $\mathcal{D}_{\mathrm{inf}}^{(\mathrm{rot})}$, is generated by infinitesimal spatial rotations C and inversion R_C of the BLG plane. The second subgroup, $\mathcal{D}_{\mathrm{inf}}^{(\mathrm{tran})}$, is generated by an infinitesimal translation t and reflection R_t. The action of these operators on the low-energy electrons is given in terms of the Pauli matrices:

$$\begin{aligned} &C \equiv i\tau_z^{AB}, \quad t \equiv i\tau_z^{KK'}, \quad R_C \equiv \tau_x^{AB}\tau_z^{KK'}, \\ &R_t \equiv \tau_z^{AB}\tau_x^{KK'}, \quad R_t \cdot R_v = \tau_y^{AB}\tau_y^{KK'}. \end{aligned} \quad \text{(A2)}$$

Note that these two groups commute with each other, unlike true translation and reflection. In the presence of the appropriate symmetry breaking these are reduced down to the $D_{3d''}$ group discussed in the text. In this case the continuous translations and rotations $\exp(\theta_t t + \theta_c C)$ become discrete with $\theta_{t,c} = 0, \pm 2\pi/3$ and the inversions R_t and R_C become $R_h \cdot R_v$ and R_v of Sec. II, respectively.

The $\mathrm{SU}(2)^{(\mathrm{spin})}$ is the group of spin rotations, which is decoupled from the physical rotations because there are no spin-orbit interactions. It is generated by rotations $\vec{S} = (S_x, S_y, S_z)$. The high-symmetry axis of any phase will always chosen to be z. Infinitesimal rotations around the z axis are represented by S_z. There are also reflections and inversion of the spin space, but these do not distinguish any phases, so we will suppress them.

The gauge groups act by multiplication. We label the infinitesimal generator g, which acts on the wave functions ψ, simply by $g\psi = i\psi$.

The time reversal operator T commutes with all of the above except the gauge generator $TgT = -g$. It is given in terms of Pauli matrices by

$$T \equiv i\sigma_y \tau_y^{KK'} \tau_y^{AB} K, \quad \text{(A3)}$$

where K is complex conjugation.

This defines the symmetry group $\mathcal{G}$ fully. A further enlarged symmetry group isomorphic to $U(1) \times U(4)$ is considered at points in the body of the text [see Eq. (2.7)] and other works, but there is no reason to expect that this will ever be an accurate approximation. We will proceed to categorize the phases according to the symmetry group $\mathcal{G}$. One may always collapse classification to obtain the distinct phases under the artificially enlarged symmetry groups.

In the following subsections we present the tables enumerating the possible symmetry breaking for the singlet, triplet, and superconducting phases each. Each table is split into subsections corresponding to the IrReps of $\mathcal{D}_{3d''}$. These are listed in the first column. At the beginning of each subsection the second column gives the order parameter (OP) for the IrRep in terms of the notation $\hat{\Delta} \equiv \Delta_{abc}\tau_a^{AB}\tau_b^{KK'}\sigma_c$ and arranges these into a vector. Next to this are the generators of symmetries under which the order parameter is invariant (generators and Δ commute). This completely characterizes one dimensional representations.

In the case of the multicomponent representations, particular values of the order parameter may have higher symmetries than the generic values—these are the distinct phases. The values of the order parameter that produce the phase are given according to the vector representation in the second column. Next to these in the third column are the additional residual symmetries under which the phase is invariant, and the phase is labeled with the additional subscript.

For example, let us take section G in the first table. The second column of first line defines a vector for the representation. The third column states that all vectors in that representation are invariant under the time T time reversal operation. The next line says that when the vector is proportional to $(1,0,0,1)$, i.e., $\Delta \propto \tau_x^{AB}\tau_x^{KK'} + \tau_y^{AB}\tau_y^{KK'}$, the symmetry is higher. The higher symmetries are in the third column; in particular, this vector is invariant under the combined $C + t$ rotation and the $R_C \cdot R_t$ reflection in addition to the T rotation. The next line of the table says that when the vector takes the value $(0,0,0,1)$ the state is invariant under the reflections R_t, R_C. Note that each phase is generally defined by

a coset of values of the order parameter, which are all invariant under conjugate groups. We only list one representative from each coset. For example, in the case of G, the $(1,0,0,1)$ vector is part of the coset of vectors $(\cos\theta, \sin\theta, -\sin\theta, \pm\cos\theta)$, $\theta \in [0,2\pi]$. These are all invariant under subgroups conjugate to the one listed in the third column.

We use α, β as arbitrary real parameters when there is a continuous manifold of cosets. When listed under symmetries the symbols t, C, g, and S_z mean the phase is invariant under the entire $U(1)$ group generated. The symbol $\vec{S}$ means the phase is invariant under all spin rotations. There are several symmetry operations involving rotations by π or $\pi/2$ in one the $U(1)$ groups. Like the spin reflections, these do not distinguish any of the phases so we do not list them. Five of the phases belonging to the G representation are illustrated in Fig. 16. Notice that, according to the Landau theory, the transition to the G-type phase cannot occur directly but rather through the pattern with incommensurate periodicity.

1. Normal phases

The normal phases are by definition invariant under spin and gauge transformation so we will suppress them. A product of Pauli matrices acting in different subspaces should be understood as a direct product. The normal phases are summarized in Table I.

TABLE I. Classification of the order parameters corresponding to distinct normal phases of BLG according to the underlying symmetry group. The structure of the table is described in the text of the Appendix.

Irr.	OP	M^α	Symmetry
A_2	Δ_{0z0}	$\tau_z^{AB}\mathbb{1}^{KK'}\mathbb{1}^N\mathbb{1}^s$	C,t,R_C
B_1	Δ_{z00}	$\mathbb{1}^{AB}\tau_z^{KK'}\mathbb{1}^N\mathbb{1}^s$	C,t,R_t
B_2	Δ_{zz0}	$\tau_z^{AB}\tau_z^{KK'}\tau_z^N\mathbb{1}^s$	$C,t,R_C\cdot R_t,T$
E_2	$(\Delta_{xz0},\Delta_{yz0})$	$\tau_{x,y}^{AB}\tau_z^{KK'}\tau_z^N\mathbb{1}^s$	t,R_C,R_t,T
E_2''	$(\Delta_{zx0},\Delta_{zx0})$	$\tau_z^{AB}\tau_{x,y}^{KK'}\tau_z^N\mathbb{1}^s$	C,R_C,R_t,T
E_1	$(\Delta_{x00},\Delta_{y00})$	$\tau_{x,y}^{AB}\mathbb{1}_z^{KK'}\mathbb{1}^N\mathbb{1}^s$	$t,R_C,R_t\cdot T$
E_1''	$(\Delta_{0x0},\Delta_{0y0})$	$\mathbb{1}^{AB}\tau_{x,y}^{KK'}\mathbb{1}^N\mathbb{1}^s$	$C,R_C,R_t\cdot T$
G	$(\Delta_{xx0},\Delta_{xy0},\Delta_{yx0},\Delta_{yy0})$	$\tau_{x,y}^{AB}\tau_{x,y}^{KK'}\tau_z^N\mathbb{1}^s$	T
G_1	$(1,0,0,1)$		$C+t,R_C\cdot R_t$
G_2	$(0,0,0,1)$		R_t,R_C

2. Magnetic phases

We restore the spin symmetries but continue to suppress the gauge symmetry. The high-symmetry axis is arbitrarily chosen to be the z direction. The magnetic phases are summarized in Table II.

TABLE II. Classification of the order parameters corresponding to distinct magnetic phases of BLG according to the underlying symmetry group. The structure of the table is described in the text of the Appendix.

Irr.	OP	M^α	Symmetry
A_1	$(\Delta_{00x},\Delta_{00y},\Delta_{00z})$	$\mathbb{1}^{AB}\mathbb{1}^{KK'}\mathbb{1}_z^N\sigma_{x,y,z}$	C,t,S_z,R_t,R_C
A_2	$(\Delta_{0zx},\Delta_{0zy},\Delta_{0zz})$	$\mathbb{1}^{AB}\tau_z^{KK'}\tau_z^N\sigma_{x,y,z}$	C,t,S_z,R_C,T
B_1	$(\Delta_{z0x},\Delta_{z0y},\Delta_{z0z})$	$\tau_z^{AB}\mathbb{1}^{KK'}\tau_z^N\sigma_{x,y,z}$	C,t,S_z,R_t,T
B_2	$(\Delta_{zzx},\Delta_{zzy},\Delta_{zzz})$	$\tau_z^{AB}\tau_z^{KK'}\mathbb{1}^N\sigma_{x,y,z}$	$C,t,S_z,R_C\cdot T,R_t\cdot T$
E_2	$(\Delta_{xzx},\Delta_{xzy},\Delta_{xzz};\Delta_{yzx},\Delta_{yzy},\Delta_{yzz})$	$\tau_{x,y}^{AB}\tau_z^{KK'}\mathbb{1}^N\sigma_{x,y,z}$	t,R_C,R_t
$E_{2,1}$	$(0,0,1;0,0,0)$		S_z
$E_{2,2}$	$(1,0,0;0,1,0)$		S_z+C
E_2''	$(\Delta_{zxx},\Delta_{zxy},\Delta_{zxz};\Delta_{zyx},\Delta_{zyy},\Delta_{zyz})$	$\tau_z^{AB}\tau_{x,y}^{KK'}\mathbb{1}^N\sigma_{x,y,z}$	C,R_C,R_t
$E_{2,1}''$	$(0,0,1;0,0,0)$		S_z
$E_{2,2}''$	$(1,0,0;0,1,0)$		S_z+t
E_1	$(\Delta_{x0x},\Delta_{x0y},\Delta_{x0z};\Delta_{y0x},\Delta_{y0y},\Delta_{y0z})$	$\tau_{x,y}^{AB}\mathbb{1}^{KK'}\tau_z^N\sigma_{x,y,z}$	t,R_t,T
$E_{1,1}$	$(0,0,1;0,0,0)$		S_z
$E_{1,2}$	$(1,0,0;0,1,0)$		S_z+C
E_1''	$(\Delta_{0xx},\Delta_{0xy},\Delta_{0xz};\Delta_{0yx},\Delta_{0yy},\Delta_{0yz})$	$\mathbb{1}^{AB}\tau_{x,y}^{KK'}\tau_z^N\sigma_{x,y,z}$	C,R_C,T
$E_{1,1}''$	$(0,0,1;0,0,0)$		S_z
$E_{1,2}''$	$(1,0,0;0,1,0)$		S_z+t
G	$(\Delta_{xxx},\Delta_{xxy},\Delta_{xxz};\Delta_{xyx},\Delta_{xyy},\Delta_{xyz};\Delta_{yxx},\Delta_{yxy},\Delta_{yxz};\Delta_{yyx},\Delta_{yyy},\Delta_{yyz})$	$\tau_{x,y}^{AB}\tau_{x,y}^{KK'}\mathbb{1}^N\sigma_{x,y,z}$	None
G_1	$(0,0,1;0,0,0;0,0,0;0,0,1)$		$S_z,C+t,R_C\cdot R_t$
G_2	$(0,0,0;0,0,0;0,0,0;0,0,1)$		S_z,R_C,R_t
G_3	$(0,0,0;1,0,0;0,0,0;0,1,0)$		S_z+t,R_C
G_4	$(0,0,0;0,0,0;1,0,0;0,1,0)$		S_z+C,R_t
G_5	$(1,0,0;0,1,0;0,-1,0;1,0,0)$		S_z+C,S_z+t

3. Superconducting phases

The order parameter M is defined by the nonzero expectation values $\langle\psi^\dagger M T \psi^\dagger\rangle$. This M is listed under OP. M must contain an even number of Pauli matrices because of fermion anticommutivity but may take complex values. The superconducting phases are summarized in Table III.

TABLE III. Classification of the order parameters corresponding to distinct superconducting phases of BLG according to the underlying symmetry group. The structure of the table is described in the text of the Appendix.

Irr.	OP	M^α	Symmetry
A_1	Δ_{000}	$\mathbb{1}^{AB}\mathbb{1}^{KK'}\tau^N_{x,y}\mathbb{1}^s$	$\vec{S},C,t,R_C,R_t,T$
A_2	$(\Delta_{0zx},\Delta_{0zy},\Delta_{0zz})$	$\mathbb{1}^{AB}\tau^{KK'}_z\tau^N_{x,y}\sigma_{x,y,z}$	C,t,R_C
$A_{2,1}$	$(0,0,1)$		S_z,T
$A_{2,2}$	$(1,i,0)$		S_z+g
B_1	$(\Delta_{z0x},\Delta_{z0y},\Delta_{z0z})$	$\tau^{AB}_z\mathbb{1}^{KK'}\tau^N_{x,y}\sigma_{x,y,z}$	C,t,R_t
$B_{1,1}$	$(0,0,1)$		S_z,T
$B_{1,2}$	$(1,i,0)$		S_z+g
B_2	Δ_{zz0}	$\tau^{AB}_z\tau^{KK'}_z\tau^N_{x,y}\mathbb{1}^s$	$\vec{S},C,t,R_C\cdot R_t,T$
E_2	$(\Delta_{xz0},\Delta_{yz0})$	$\tau^{AB}_{x,y}\tau^{KK'}_z\tau^N_{x,y}\mathbb{1}^s$	$\vec{S},t,R_C,R_t$
$E_{2,1}$	$(1,0)$		T
$E_{2,2}$	$(1,i)$		$C+g$
E''_2	$(\Delta_{zx0},\Delta_{zy0})$	$\tau^{AB}_z\tau^{KK'}_{x,y}\tau^N_{x,y}\mathbb{1}^s$	$\vec{S},C,R_C,R_t$
$E''_{2,1}$	$(1,0)$		T
$E''_{2,2}$	$(1,i)$		$t+g$
E_1	$(\Delta_{x0x},\Delta_{x0y},\Delta_{x0z};\Delta_{y0x},\Delta_{y0y},\Delta_{y0z})$	$\tau^{AB}_{x,y}\mathbb{1}^{KK'}\tau^N_{x,y}\sigma_{x,y,z}$	t
$E_{1,1}$	$(0,0,1;0,0,0)$		S_z,R_C,T
$E_{1,2}$	$(1,i,0;0,0,0)$		$S+g,R_C$
$E_{1,3}$	$(0,0,1;0,0,i)$		$S_z,C+g,R_C\cdot T$
$E_{1,4}$	$(\alpha,i\alpha,i\beta;i\alpha,-\alpha,\beta)$		$C+S+2g$
$E_{1,5}$	$(1,i,0;i,-1,0)$		$C+g,S+g$
E''_1	$(\Delta_{0xx},\Delta_{0xy},\Delta_{0xz};\Delta_{0yx},\Delta_{0yy},\Delta_{0yz})$	$\mathbb{1}^{AB}\tau^{KK'}_{x,y}\tau^N_{x,y}\sigma_{x,y,z}$	C
$E''_{1,1}$	$(0,0,1;0,0,0)$		S_z,R_t,T
$E''_{1,2}$	$(1,i,0;0,0,0)$		$S+g,R_t$
$E''_{1,3}$	$(0,0,1;0,0,i)$		$S_z,t+g,R_C\cdot T$
$E''_{1,4}$	$(\alpha,i\alpha,i\beta;i\alpha,-\alpha,\beta)$		$t+S+2g$
$E''_{1,5}$	$(1,i,0;i,-1,0)$		$t+g,S+g$
G	$(\Delta_{xx0},\Delta_{xy0},\Delta_{yx0},\Delta_{yy0})$	$\tau^{AB}_{x,y}\tau^{KK'}_{x,y}\tau^N_{x,y}\mathbb{1}^s$	None
G_1	$(1,0,0,1)$		$C+t,R_C\cdot R_t,T$
G_2	$(0,0,0,1)$		R_C,R_t,T
G_3	$(0,0,-i,1)$		$C+g,R_C,R_t\cdot T$
G_4	$(0,-i,0,1)$		$t+g,R_t,R_C\cdot T$
G_5	$(1,i,i,-1)$		$C+g,t+g,R_C\cdot R_t\cdot T$

[1] E. McCann and V. I. Fal'ko, Phys. Rev. Lett. **96**, 086805 (2006).
[2] K. S. Novoselov, E. McCann, S. V. Morozov, V. I. Falko, M. I. Katsnelson, U. Zeitler, D. Jiang, F. Schedin, and A. K. Geim, Nat. Phys. **2**, 177 (2006).
[3] R. Nandkishore and L. Levitov, Phys. Rev. Lett. **104**, 156803 (2010).
[4] J. Jung, F. Zhang, and A. H. MacDonald, Phys. Rev. B **83**, 115408 (2011).
[5] M. Kharitonov, arXiv:1109.1553.
[6] H. Min, G. Borghi, M. Polini, and A. H. MacDonald, Phys. Rev. B **77**, 041407(R) (2008).
[7] F. Zhang, J. Jung, G. A. Fiete, Q. Niu, and A. H. MacDonald, Phys. Rev. Lett. **106**, 156801 (2011).
[8] O. Vafek, Phys. Rev. B **82**, 205106 (2010).
[9] R. Nandkishore and L. Levitov, Phys. Rev. B **82**, 115124 (2010).
[10] H. Dahal, T. Wehling, K. Bedell, J. Zhu, and A. V. Balatsky, Physica B **405**, 2241 (2010).
[11] F. Zhang, H. Min, M. Polini, and A. H. MacDonald, Phys. Rev. B **81**, 041402(R) (2010).
[12] L. Zhu, V. Aji, and C. Varma, arXiv:1202.0821.
[13] Y. Lemonik, I. L. Aleiner, C. Toke, and V. I. Fal'ko, Phys. Rev. B **82**, 201408 (2010).
[14] O. Vafek and K. Yang, Phys. Rev. B **81**, 041401(R) (2010).
[15] B. Feldman, J. Martin, and A. Yacoby, Nat. Phys. **5**, 889 (2009).
[16] R. T. Weitz, M. T. Allen, B. E. Feldman, J. Martin, and A. Yacoby, Science **330**, 812 (2010).

[17] A. S. Mayorov, D. C. Elias, M. Mucha-Kruczynski, R. V. Gorbachev, T. Tudorovskiy, A. Zhukov, S. V. Morozov, M. I. Katsnelson, V. I. Fal'ko, A. K. Geim, and K. S. Novoselov, Science **333**, 860 (2011).

[18] J. Velasco Jr., L. Jing, W. Bao, Y. Lee, P. Kratz, V. Aji, M. Bockrath, C. N. Lau, C. Varma, R. Stillwell, D. Smirnov, Fan Zhang, J. Jung, and A. H. MacDonald, Nat. Nanotechnol. **7**, 156 (2012).

[19] F. Freitag, J. Trbovic, M. Weiss, and C. Schonenberger, Phys. Rev. Lett. **108**, 076602 (2012).

[20] W. Bao *et al.*, arXiv:1202.3212.

[21] A. Veligura, H. J. van Elferen, N. Tombros, J. C. Maan, U. Zeitler, and B. J. van Wees, Phys. Rev. B **85**, 155412 (2012).

[22] T. Ohta, A. Bostwick, T. Seyller, K. Horn, and E. Rotenberg, Science **313**, 5789 (2006).

[23] E. A. Henriksen, Z. Jiang, L.-C. Tung, M. E. Schwartz, M. Takita, Y.-J. Wang, P. Kim, and H. L. Stormer, Phys. Rev. Lett. **100**, 087403 (2008).

[24] L. M. Zhang, Z. Q. Li, D. N. Basov, M. M. Fogler, Z. Hao, and M. C. Martin, Phys. Rev. B **78**, 235408 (2008).

[25] Z. Q. Li, E. A. Henriksen, Z. Jiang, Z. Hao, M. C. Martin, P. Kim, H. L. Stormer, and D. N. Basov, Phys. Rev. Lett. **102**, 037403 (2009).

[26] A. B. Kuzmenko, I. Crassee, D. van der Marel, P. Blake, and K. S. Novoselov, Phys. Rev. B **80**, 165406 (2009).

[27] A. B. Kuzmenko, E. van Heumen, D. van der Marel, P. Lerch, P. Blake, K. S. Novoselov, and A. K. Geim, Phys. Rev. B **79**, 115441 (2009).

[28] M. Mucha-Kruczynski, I. L. Aleiner, and V. I. Fal'ko, Phys. Rev. B **84**, 041404 (2011).

[29] D. T. Son, Phys. Rev. B **75**, 235423 (2007).

[30] I. L. Aleiner, D. E. Kharzeev, and A. M. Tsvelik, Phys. Rev. B **76**, 195415 (2007).

[31] J. E. Drut and D. T. Son, Phys. Rev. B **77**, 075115 (2008).

[32] D. M. Basko, Phys. Rev. B **78**, 125418 (2008).

[33] Y. Lemonik and I. Aleiner (unpublished).

[34] For generic choices of the coupling constants these interactions reduce the symmetry of the model from the artificial SU(4) $\otimes$ $U(1)$ $\otimes$ $U(1)$ down to SU(2) $\otimes$ $U(1)$ $\otimes$ $U(1)$ $\otimes$ $\mathcal{D}_{3d}$. This is still larger than the original symmetry group as $\tau_z^{KK'}$ does not generate continuous rotations in the original space group. The continuous $\tau_z^{KK'}$ rotation is broken by umklapp terms down to Z_3. However, the lowest order umklapp term is of the form $H_{\text{umklapp}} \sim (\psi^\dagger \tau_+^{KK'} \tau_z^{AB} \psi)^3 +$ H.c. Since this contains six fermion creation and annihilation operators it will be strongly RG irrelevant and we will not consider it.

[35] Equations (3.12) and (3.13) appeared in Ref. 13 with several typos. Furthermore, a misdefinition of ℓ led to incorrect statements on the critical temperature of nematic state. The errors have been corrected in the present paper.

[36] S. Coleman, *Aspects of Symmetry* (Cambridge University Press, New York, 1985).

[37] In the body of this paper the case of BLG with $N = 1$ fermion flavors is discussed. This is not a case of physical interest. In an unpublished appendix to arXiv:0907.2448 they list RG equations for ten independent couplings. This contradicts the symmetry analysis of this paper which demonstrates there can be only nine independent couplings. Further, the set of interactions chosen violates SU(2) spin rotational invariance, a fact which is not noted. Note that only requiring invariance under spin rotations in the BLG plane requires 13 independent parameters, so this does not explain the claims of Ref. 11.

[38] M. M. Scherer, S. Uebelacker, and C. Honerkamp, arXiv:1112.5038.

[39] Y. Lemonik, I. Aleiner, and V. Fal'ko (unpublished).

[40] C. L. Kane and E. J. Mele, Phys. Rev. Lett. **95**, 226801 (2005).